AD-A133 753 RESULTS FROM A TWO-LAYER AND A REDUCED GRAVITY MODEL OF 1/1
THE ALBORAN SEA(U) A. (U) JAYCOR ALEXANDRIA VA
R H PRELLER 12 SEP 83 JAYCOR-J206-83-009/6226
UNCLASSIFIED N00014-82-C-0761 F/G 8/10 NL

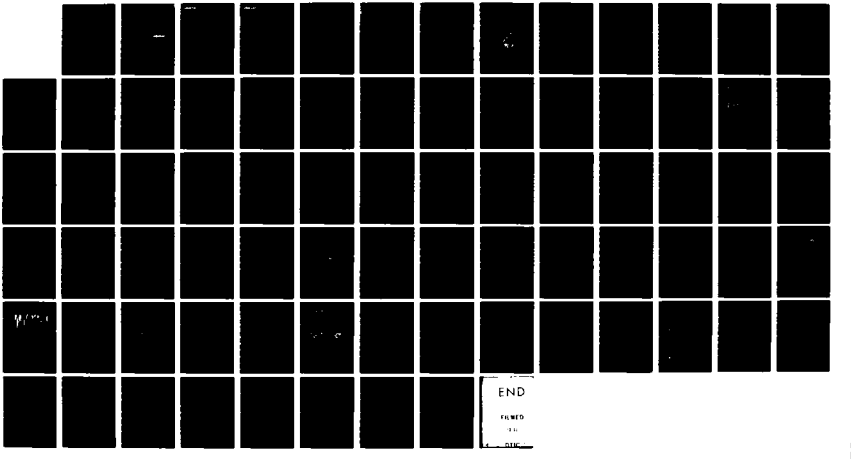

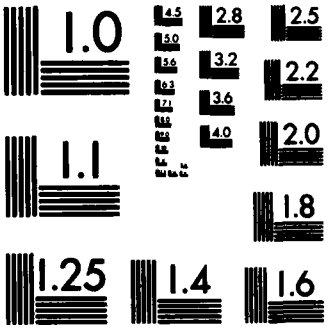

MICROCOPY RESOLUTION TEST CHART
NATIONAL BUREAU OF STANDARDS-1963-A

(12)

RESULTS FROM A TWO-LAYER AND A REDUCED GRAVITY MODEL OF THE ALBORAN SEA; AND VERTICAL SHEAR FROM TOPS

J206-83-009/6226

JAYCOR

83 09 14 013

205 South Whiting Street
Alexandria, Virginia 22304

JAYCOR

RESULTS FROM A TWO-LAYER AND A REDUCED GRAVITY MODEL OF THE ALBORAN SEA; AND VERTICAL SHEAR FROM TOPS

J206-83-009/6226

Final Report

by

Ruth H. Preller

September 12, 1983

Prepared for:

Naval Ocean Research and Development Activity
NSTL Station, MS 39529

Under:

Contract Number N00014-82-C-0761

205 South Whiting Street • Alexandria, Virginia 22304 • (703) 823-1300

JAYCOR

6226

September 12, 1983

Dr. Steven A. Piacsek
NORDA
Code 322
NSTL Station, MS 39529

SUBJECT: Final Report, Contract Number N00014-82-C-0761.

Dear Dr. Piacsek:

JAYCOR is pleased to submit this Final Report entitled, *Results from a Two-Layer and a Reduced Gravity Model of the Alboran Sea; and Vertical Shear from TOPS*, in accordance with the subject contract, CDRL Item Number A002.

If the Final Report is acceptable, please sign and forward the enclosed DD Form 250.

Questions of a technical nature should be addressed to Dr. Alan Wallcraft or Ms. Ruth Preller while questions of a contractual nature should be addressed to the undersigned.

We have enjoyed working with you and look forward to a continuing relationship.

Sincerely,

Martin C. Nielsen
Manager of Administration
and Counsel

ssh-b

Enclosures

cc: Administrative Contracting Officer, Code 621
Director, NRL, Code 2627
Defense Technical Information Center

205 South Whiting Street • Alexandria, Virginia 22304 • (703) 823-1300

UNCLASSIFIED

SECURITY CLASSIFICATION OF THIS PAGE (When Data Entered)

REPORT DOCUMENTATION PAGE	READ INSTRUCTIONS BEFORE COMPLETING FORM
1. REPORT NUMBER: J206-83-009/6226	2. GOVT ACCESSION NO.: AD-A133753
3. RECIPIENT'S CATALOG NUMBER	
4. TITLE (and Subtitle): RESULTS FROM A TWO-LAYER AND A REDUCED GRAVITY MODEL OF THE ALBORAN SEA; AND VERTICAL SHEAR FROM TOPS	5. TYPE OF REPORT & PERIOD COVERED: Final Report 08/03/82 thru 05/12/83
	6. PERFORMING ORG. REPORT NUMBER: J206-83-009/6226
7. AUTHOR(s): Ruth H. Preller	8. CONTRACT OR GRANT NUMBER(s): N00014-82-C-0761
9. PERFORMING ORGANIZATION NAME AND ADDRESS: JAYCOR, 205 South Whiting Street, Alexandria, VA 22304	10. PROGRAM ELEMENT, PROJECT, TASK AREA & WORK UNIT NUMBERS: A002
11. CONTROLLING OFFICE NAME AND ADDRESS: Naval Ocean Research and Development Activity, NSTL Station, MS 39529	12. REPORT DATE: September 12, 1983
	13. NUMBER OF PAGES: 71 pages
14. MONITORING AGENCY NAME & ADDRESS(if different from Controlling Office)	15. SECURITY CLASS. (of this report): UNCLASSIFIED
	15a. DECLASSIFICATION/DOWNGRADING SCHEDULE

16. DISTRIBUTION STATEMENT (of this Report)

1 - Scientific Officer
1 - Administrative Contracting Officer, Code 621
6 - Director, NRL Code 2627
12 - Defense Technical Information Center

17. DISTRIBUTION STATEMENT (of the abstract entered in Block 20, if different from Report)

18. SUPPLEMENTARY NOTES

19. KEY WORDS (Continue on reverse side if necessary and identify by block number)

Alboran Sea, Alboran gyre, Strait of Gibraltar, vertical shear, Richardson number, Synthetic Bathymetric Profiling System (SYNBAPS), Thermodynamic Ocean Prediction System (TOPS).

20. ABSTRACT (Continue on reverse side if necessary and identify by block number)

DD FORM 1 JAN 73 1473 EDITION OF 1 NOV 65 IS OBSOLETE
S/N 0102-LF-014-6601

UNCLASSIFIED
SECURITY CLASSIFICATION OF THIS PAGE (When Data Entered)

TABLE OF CONTENTS

RESULTS FROM A TWO LAYER AND A REDUCED GRAVITY MODEL OF THE ALBORAN SEA

INTRODUCTION

The circulation of the Alboran Sea is dependent on both Atlantic and Mediterranean waters. Atlantic water flows through the narrow (20 km wide) and shallow (300 m deep) Strait of Gibraltar into the Alboran Sea forming a 150-200 m deep surface layer (Ovchinnikov, 1966; Lanoix, 1974; Katz, 1972). Mediterranean water enters the Alboran at its open eastern boundary and flows slowly westward in the form of an intermediate and lower layer. It has been suggested that even the deepest water can exit through the Strait (Stommel et al., 1973). The large volume transport of inflowing Atlantic water, 1 to 2 X 10^6 m^3/sec, (Lacombe, 1971; Bethoux, 1979; Lacombe, 1982) retains its identity as a narrow (30 km wide) jet with initial speeds of 100 cm/sec near the Strait (Lacombe, 1961; Peluchon and Donguy, 1962; Grousson and Faroux, 1963; Lanoix, 1974; Cheney, 1977; Petit et al., 1978; and Wannamaker, 1979). The jet enters the basin and flows northeast to approximatley 4°W, curves southward and then splits (Figure 1). Part of the jet flows to the west and is incorporated in an anticyclonic gyre, while the remainder flows southeast to Cape Tres Forcas and then along the African coast forming the southern periphery of a cylconic circulation.

Satellite infrared imagery indicates variations in the shape, location and intensity of the persistent anticylconic gyre which dominates the western Alboran Sea. Hydrographic data and satellite infrared images support the year-round persistence of the gyre, although its size and location varies (Stevenson, 1977; Cheney, 1978; Wannamaker, 1979; Burkov et al., 1979; Gallagher et al., 1981). In the eastern portion of the Alboran Sea a general pattern of alternating cyclonic and anticyclonic circulations has been observed (Cheney, 1978; Lanoix, 1974). Satellite imagery shows that, compared to the western Alboran, this circulation pattern is far more variable and of smaller scale.

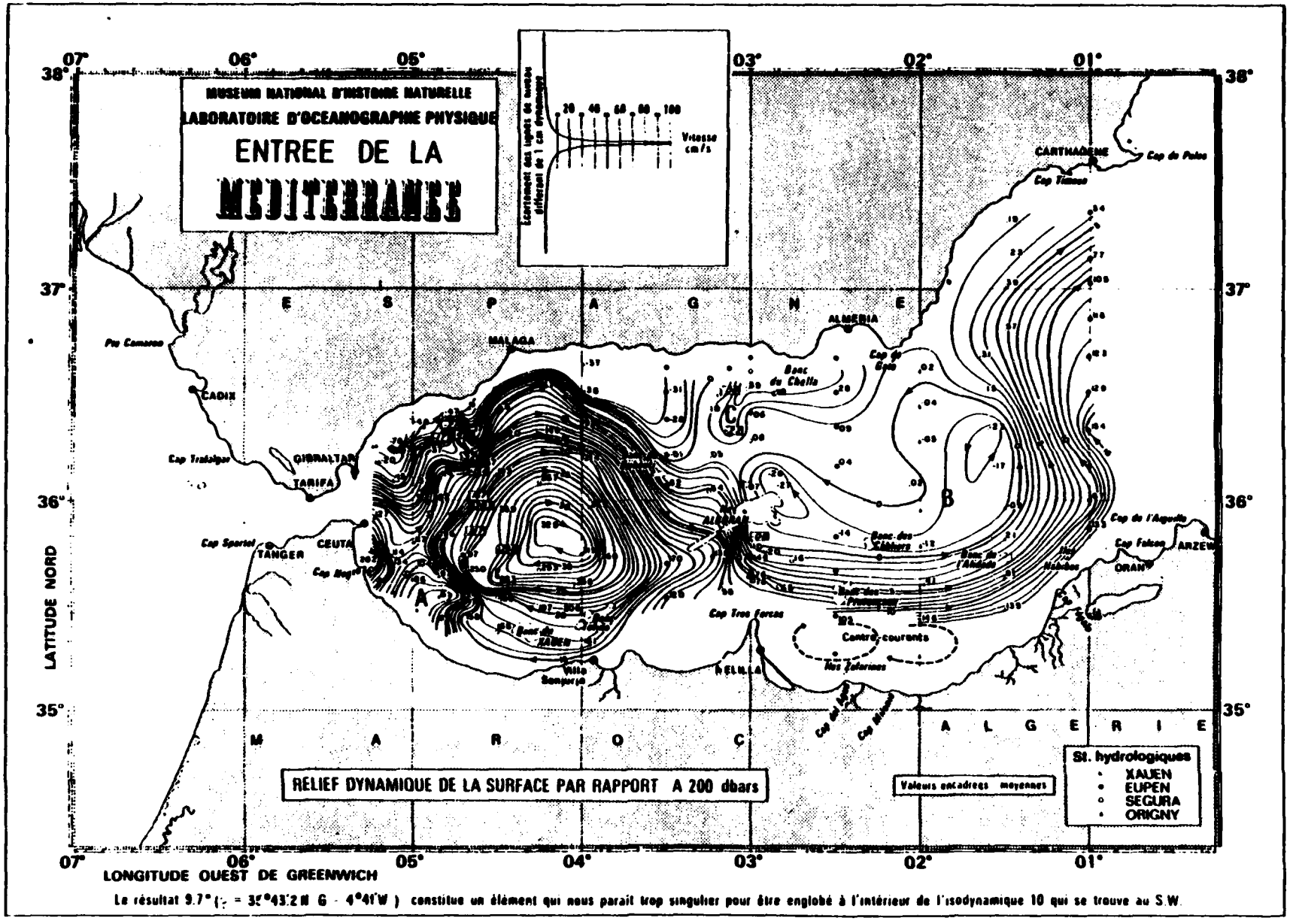

Le résultat 9.7° (= 35°43'2 N G - 4°41'W) constitue un élément qui nous paraît trop singulier pour être englobé à l'intérieur de l'isodynamique 10 qui se trouve au S.W.

Figure 1. Dynamic topography of the surface relative to 200 dbar for July-August 1962. Lanov (1974).

A study of circulation in the Alboran Sea begins by using the simplest model capable of simulating major features of the circulation. In a system with two so clearly defined layers, a reduced gravity model may be used to determine the circulation of the upper layer, and a two layer model to determine the entire system. The reduced gravity model allows baroclinic instability and the inclusion of bottom topography. Previous results using a semi-implicit reduced gravity model with a rectangular geometry are discussed in Preller and Hurlburt, (1982). We have now progressed to a reduced gravity model with real geometry and a two layer model with geometry and bottom topography.

THE MODEL

The non-linear reduced gravity and two layer models, developed for the Gulf of Mexico by Hurlburt and Thompson, (1980), have been adapted and modified for the Alboran Sea. The reduced gravity model is an explicit variant of the Hurlburt and Thompson model and is described in detail by Preller and Heburn, (1983). The two layer model is solved numerically using the economic semi-implicit method. The reduced gravity model consists of an active upper layer and a lower layer which is infinitely deep and at rest. The two layer model has an upper layer, a finite lower layer and may include bottom topography (Figure 2). Both models are stably stratified and have a fixed density contrast between two immiscible layers. These models assume a hydrostatic, Boussinesq fluid in a rotating right-handed coordiniate system on a -plane. The vertically integrated model equations are:

$$\frac{\partial \vec{V}_i}{\partial t} + (\nabla \cdot \vec{V}_i + \vec{V}_i \cdot \nabla)\,\vec{v}_i + \hat{k} \times f\vec{V}_i = h_i \nabla P_i + (\vec{\tau}_1 - \vec{\tau}_2)/\rho + A\nabla^2\vec{V}_i$$

$$\frac{\partial h_i}{\partial t} + \nabla \cdot \vec{V}_i = 0$$

where

$$\nabla = \frac{\partial}{\partial x}\hat{i} + \frac{\partial}{\partial y}\hat{j}$$

$$P_1 = g\eta$$

$$P_2 = P_1 - g'h_1$$

$$\vec{V}_i = h_i\vec{v}_i = h_i\,(u_i\hat{i} + v_i\hat{j})$$

$$g' = g(\rho_2 - \rho_1)/\rho$$

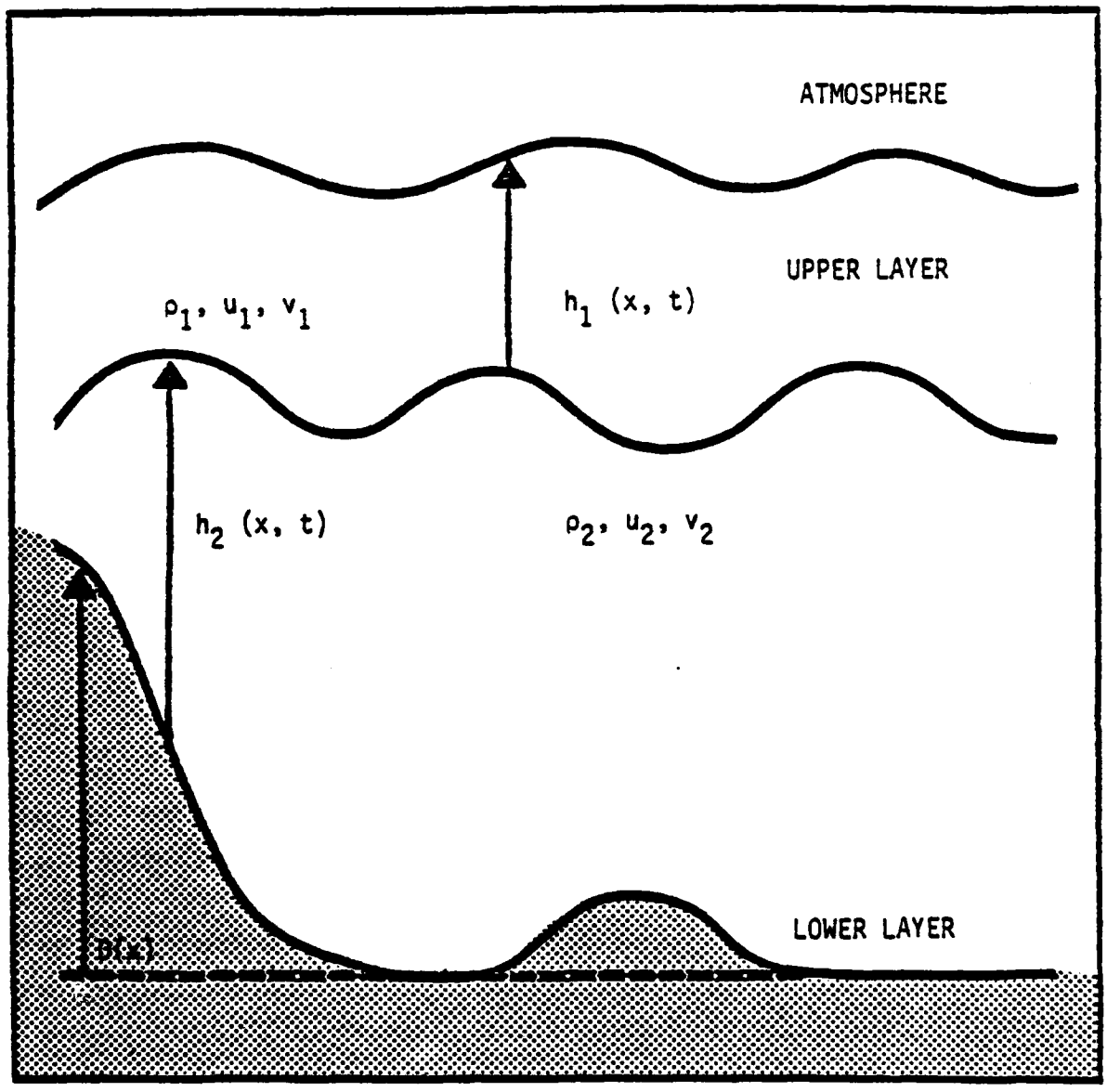

Figure 2. Two layer model cross section.

$$f = f_0 + \beta (y - y_0)$$

$$\tau_i = \tau_i^x \hat{i} + \tau_i^y \hat{j}$$

$i = 1, 2$ indicates upper and lower layers

and x and y are tangent-plane Cartesian coordinates with x directed eastward and y northward, u_i and v_i are the eastward and northward velocity components in each layer, h_i is the thickness of each layer, t is time, g is the acceleration due to gravity, ρ_i is the density of seawater in layer i, f_0 and y_0 are the values of the Coriolis parameter and the y-coordinate at the southern boundary, $\vec{\tau}_1$ is the wind stress, and $\vec{\tau}_2$ is the interfacial stress.

Figure 3 depicts the irregular geometry and topography used in the two layer experiments and the explicit reduced gravity cases. This irregular boundary was created from the Synthetic Bathymetric Profiling System (SYNBAPS) (Vanwyckhouse, 1973 and Vanwyckhouse, 1979) data set of topography. These values were interpolated from the 10 minute resolution of the model. The coastline was then drawn using a cutoff depth of 20 m to eliminate errors existing on the boundary of the data set. The four point island in the center of the basin is an idealized representation of the Alboran Island. A four point island, 20 km X 10 km, is the smallest allowed by the numerical schemes used in the model. Except at the ports, boundaries are rigid and a no slip boundary condition is prescribed on the tangential flow. Velocity is prescribed at the inflow port. Normal flow at the outflow port is self-determined with the integral constraint that the total transport out of each layer match the inflow. In the two layer cases, the amplitude of the tangential component was set to zero one-half the grid distance outside the physical domain at both ports. A variation of the Orlanski boundary condition (see Preller and Heburn, 1983) was used on outflow in the explicit reduced gravity model.

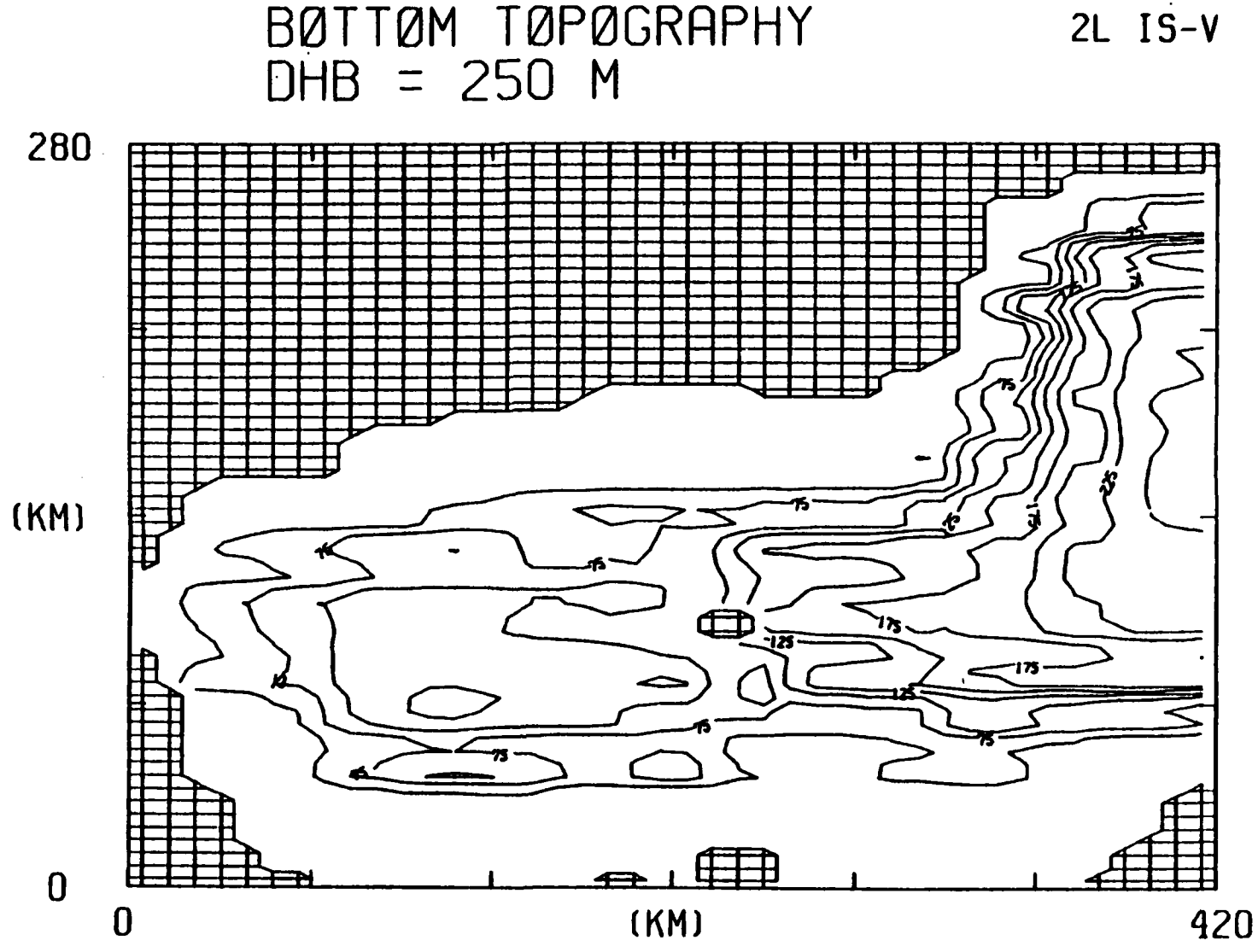

Figure 3. Geometry and topography of the Alboran Sea based on SYNBAPS data.

Model parameters for each of the model's standard cases are given in Table 1. The only dissipation in the model, other than the viscous boundary layer, is due to horizontal friction. The value for the coefficient of eddy viscosity was chosen to keep the grid interval Reynolds number

$$Re = \frac{V\Delta X}{A} \approx 30,$$

thus keeping the effects of frictional damping from dominating the solutions.

The value chosen for reduced gravity due to stratification was appropriate for observed density differences in the Alboran Sea. In the two layer model, the value of g' in the table is multiplied by $(H_1 + H_2)/H_2$ to yield the same internal values for gravity wave speed, radius of deformation and Rossby wave speed as in the reduced gravity model. The undisturbed upper layer thickness is based on many observations of the Alboran Sea which show a sharp density-salinity gradient at 150-200 m depth.

Horizontal grid spacing was chosen to allow the resolution of the mesoscale features being studied in the Alboran Sea. A minimum of 8-10 grid points is necessary to properly resolve a feature. The Alboran Gyre is defined with an average diameter of 100 km. Thus the model has a minimum of 10 grid points with which to define this feature.

For cases using the irregular geometry, the western inflow port is 20 km wide, an appropriate width for the Strait of Gibraltar, while the eastern outflow port is 245 km wide. In the lower layer of the two layer cases, the eastern boundary serves as the inflow port while the Strait of Gibraltar becomes the outflow boundary. Inflow is exactly compensated by outflow separately in each layer. Specification of the model forcing is accomplished using one of two methods:

- By prescribing velocity, (v_{1in}), or

Table 1

MODEL PARAMETERS FOR THE PIVOTAL EXPERIMENT

Parameter	Definition	Value
A	eddy viscosity	$150\ m^2\ sec^{-1}$
β	(df/dy)	$2 \times 10^{-11} m^{-1} sec^{-1}$
f_o	Coroilis parameter	$8 \times 10^{-5} sec^{-1}$
g'	reduced gravity due to stratification	$.02\ m\ sec^{-2}$
H_1	undisturbed upper layer depth	200 m
H_2	undisturbed lower layer depth	
	reduced gravity	∞
	2 layer	2400 m
$L_x \times L_y$	horizontal dimensions of the model domain	420 km x 280 km
$\Delta x \times y$	horizontal grid spacing for each dependent variable	10 km x 5 km
Δt	time step reduced gravity	900 sec
	2 layer	2700 sec
$\vec{v}_{1in}$	upper layer inflow velocity	30 cm/sec
$\vec{v}_{2in}$	lower layer inflow velocity	.2 cm/sec
α	angle of inflow	21° north of east
t_s	inflow spin up time constant	30 days

- by prescribing transport, (V_{1in}), and allowing the model to determine the velocities.

Using a standard inflow velocity of 30 cm/sec through a 20 km wide 200 m deep port determines an inflow transport of 1.2 x 10^6 m/sec or (10^6 m/sec = 1 sv) 1.2 sverdrups. This value is centered within the limits of the observed transport. A standard inflow value of .2 cm/sec was chosen for the lower layer to agree with observation. Transport out of the Mediterranean is known to be less then incoming transport due to the effect of evaporation being greater than precipitation. An inflow of .2 cm/sec through a 245 km wide boundary which is a maximum of 2400 m deep creates a mass transport of 1.1 sv. It also creates velocities along the southern shelf near the Strait of Gibraltar of 10 cm/sec. This also agrees with observation (personal communication - J.C. Gascard). Inflow is spun up with a time constant of thirty days to minimize excitation of high frequency waves. The standard ar e of inflow was chosen to be 21 north of east based on the geometric orientation of the Strait of Gibraltar. This angle was varied based on direct observations (Lacombe, 1961) and inferences from satellite imagery.

The wind forcing is derived from climatological wind stresses obtained from twenty years (1950-1970) of ship observations in the Mediterranean (May 1982). Individual stresses were estimated from ship observations of wind speed and direction using a quadratic aerodynamic drag law with a drag coefficient dependent on the wind speed and stability. Monthly averages of the wind stresses were then calculated by averaging the individual wind stress estimates from each month on a one degree latitude by one degree longitude grid. These monthly averages were bilinearly interpolated to the model grid (Figures 4, 5 and 6). Wind forcing in the model is cyclic with a period of one year.

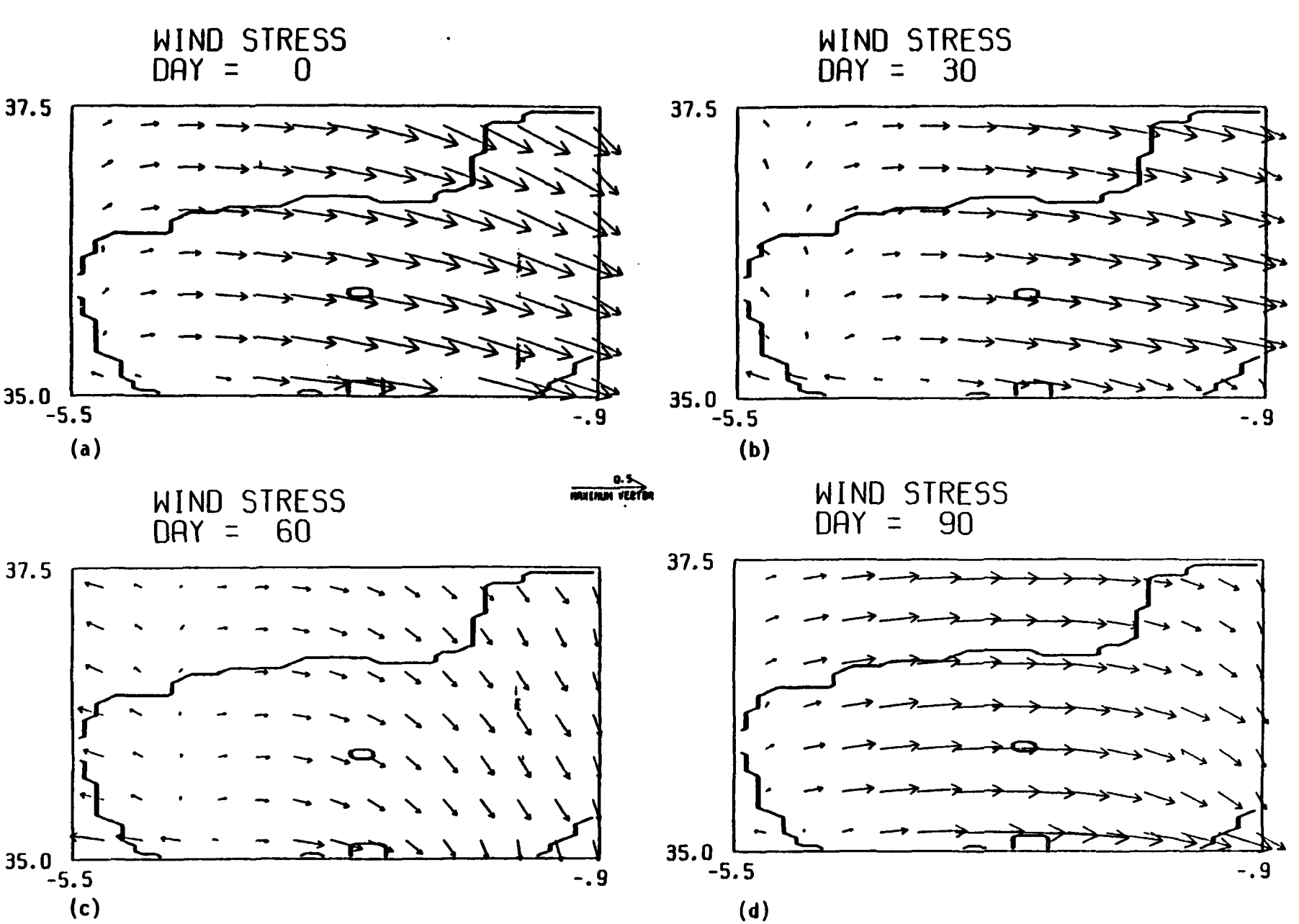

Figure 4. Monthly mean climatological wind stress for (a) January, (b) February, (c) March and (d) April.

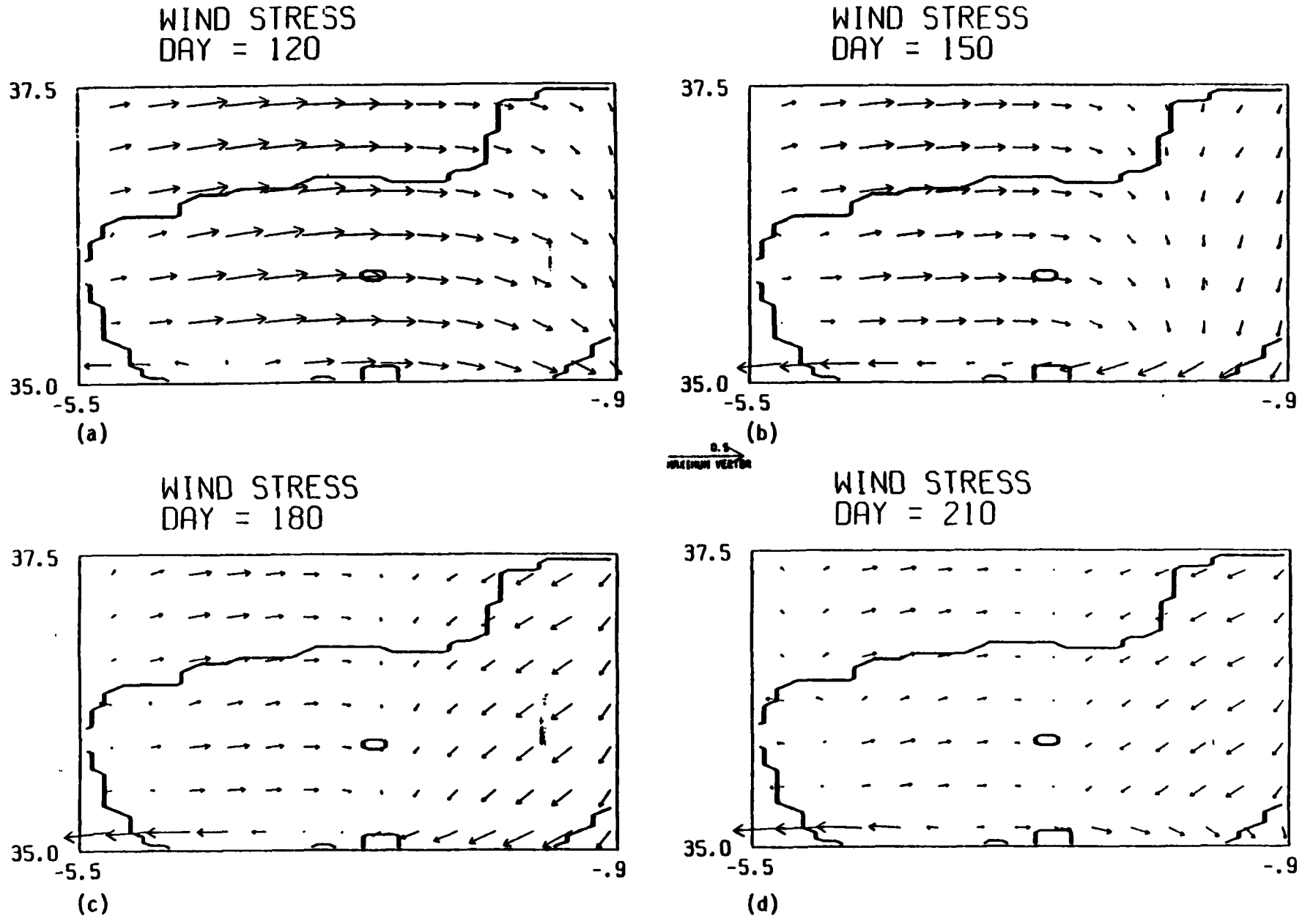

Figure 5. Monthly mean climatological wind stress for (a) May, (b) June, (c) July and (d) August.

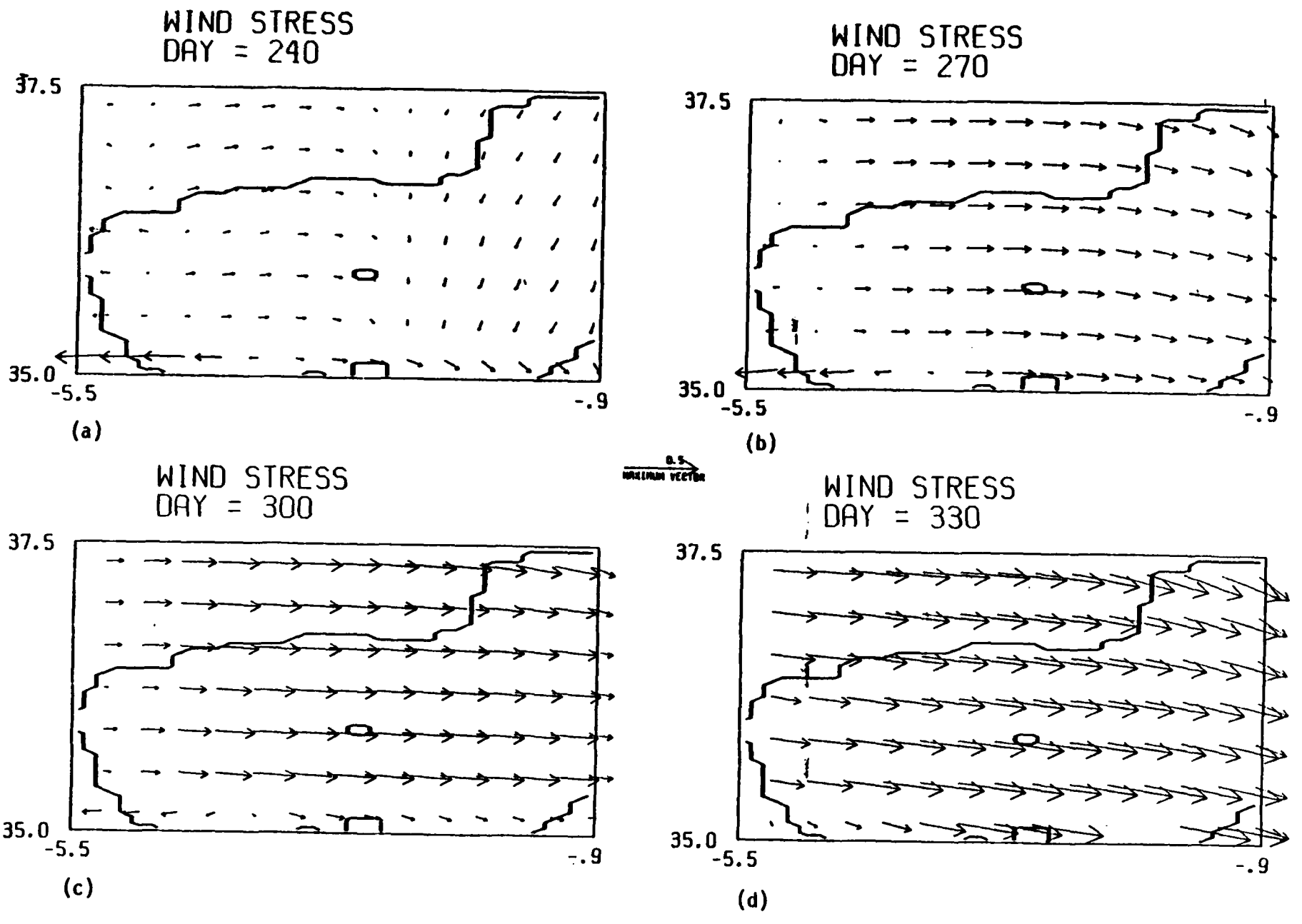

Figure 6. Monthly mean climatological wind stress for (a) September, (b) October, (c) November and (d) December.

MODEL RESULTS

Model results will be presented first in terms of two layer results then explicit reduced gravity results. The numerical solutions presented have evolved out to a steady state.

The pivotal two layer experiment used the parameters of Table 1. All solutions are presented in terms of pynocline height anomaly (PA) the deviation of the interface between the upper and lower layers from its initial rest position at 200 m depth. Solid contours indicate a deepening of the layer while dashed contours indicated a shallowing of the layer. Closed solid contours represent regions of anticyclonic circulation while closed dashed contours are regions of cyclonic circulation . Figure 7a shows the steady state solution of the pivotal case. The dominant feature observed is an anticyclonic gyre representing the Alboran gyre occupying almost the entire western half of the basin. This solution is quite similar to the semi-implicit reduced gravity model solutions discussed by Preller and Hurlburt, 1982 (Figure 7b). The addition of a slowly moving lower layer seems to have very little effect on the solutions. Figure 8 shows the lower layer velocity field for the pivotal case. Though flow enters the basin uniformly, it is quickly steered by the topography to the southern shelf and then exits through the Strait of Gibraltar. Although the velocity field has a clearly defined pattern, magnitudes still remain very small (< 10 cm/sec).

A more important effect seems to be the coastal feature, Cape Tres Forcas and the Alboran Island. Figure 9a shows the steady state two layer solution when inflow is prescribed due east. Cape Tres Forcas serves to deflect the jet, not allowing it to abruptly hit the southern boundary. This is brought out clearly by the semi-implicit reduced gravity solution, Figure 9b, which uses rectangular geometry. The jet, in this case, hits the flat wall and turns sharply upward enhancing the cyclonic circulation north of the jet.

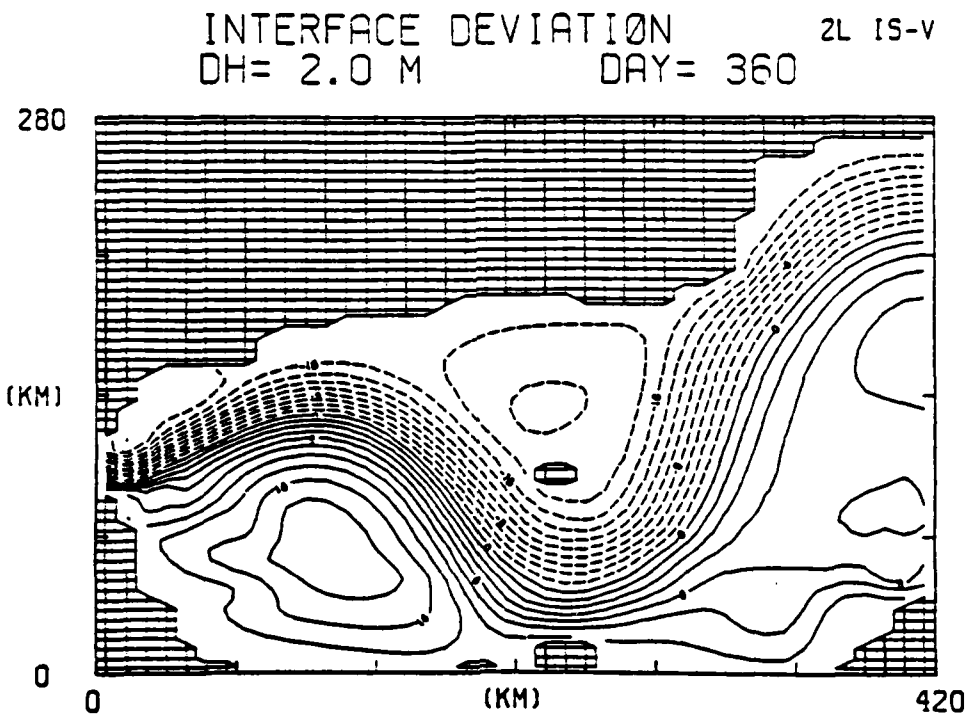

Figure 7a. PA (pynocline anomaly) of the two layer case with the Alboran Isle. Inflow angle is 21° and inflow magnitude is 30 cm/sec. Contours run from +20 to -20 meters with a contour interval of 2 m.

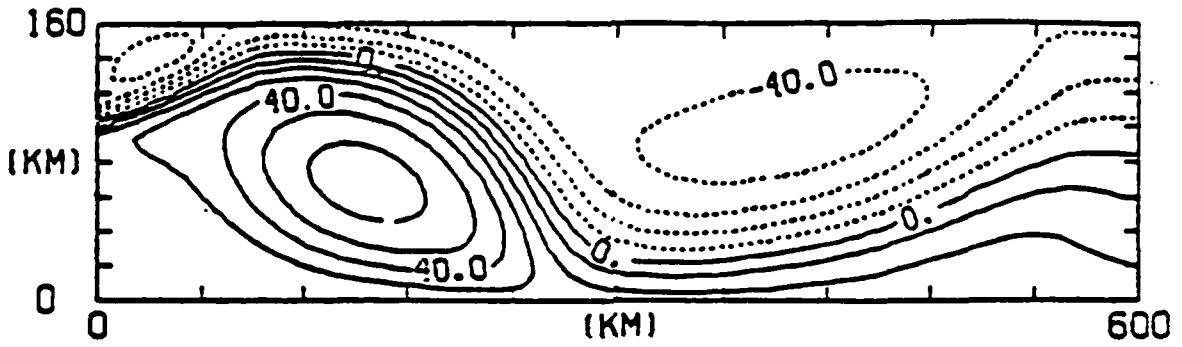

Figure 7b. PA of the reduced gravity case at day 500. Inflow angle is 21° north of east. Solid contours are positive (downward) deviations. Dashed contours are negative (upward) deviations. Contour interval is 10 m.

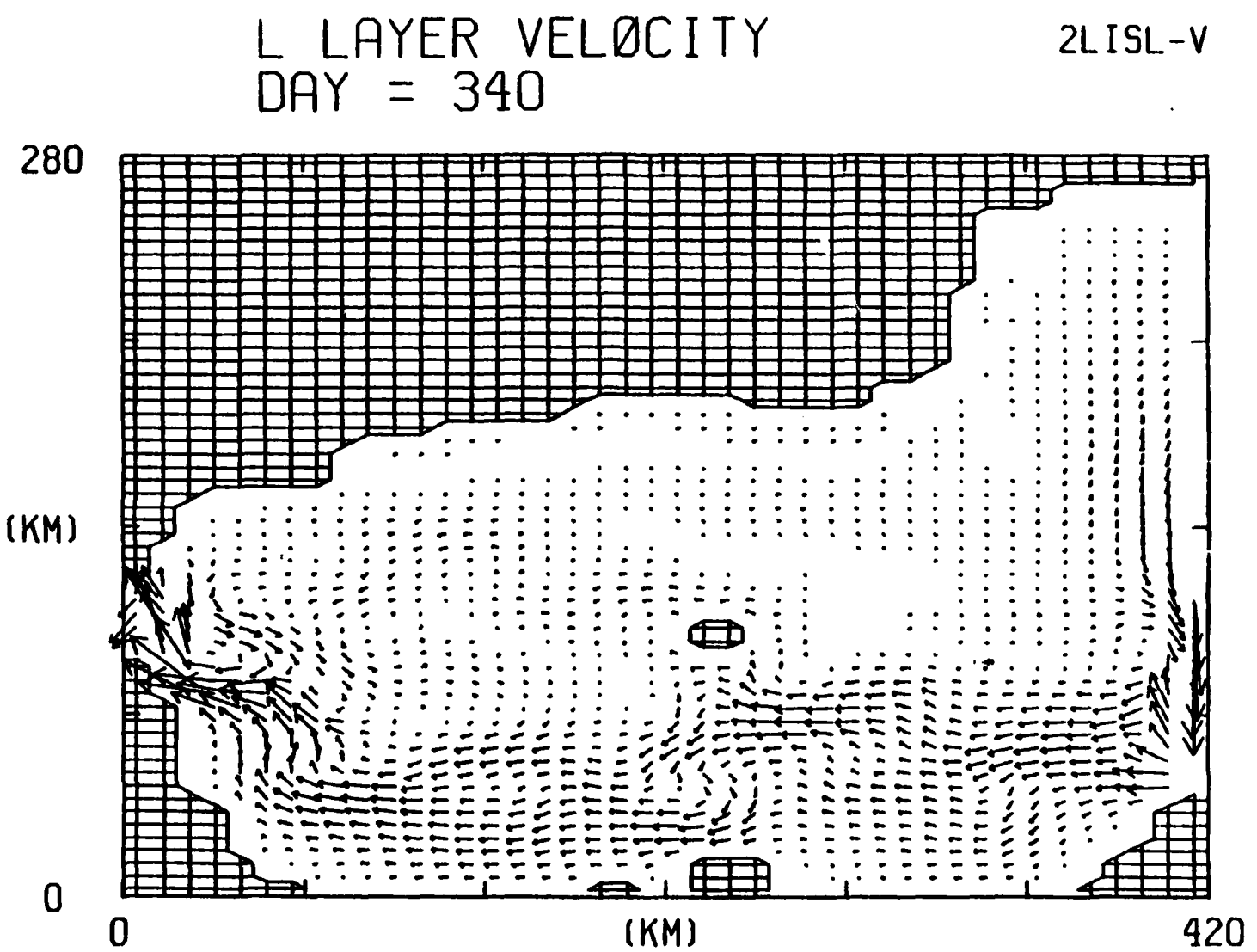

Figure 8. Lower layer velocity field for the pivotal case.

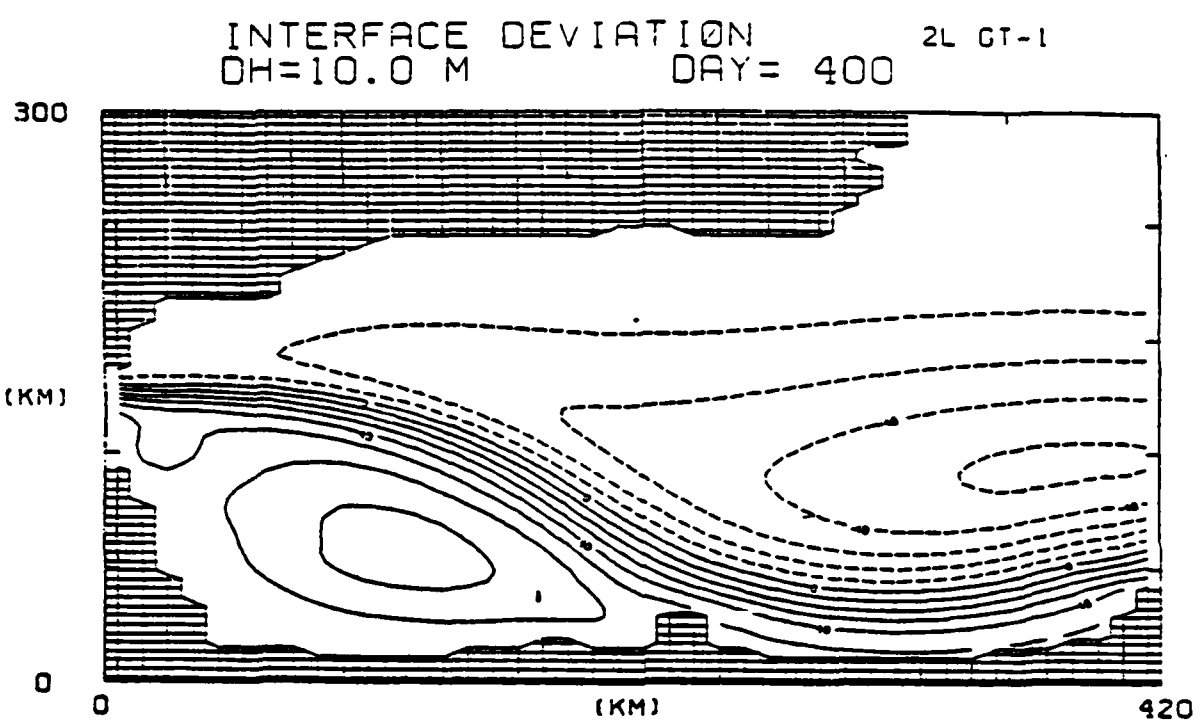

Figure 9a. Two layer solution with prescribed due east inflow.

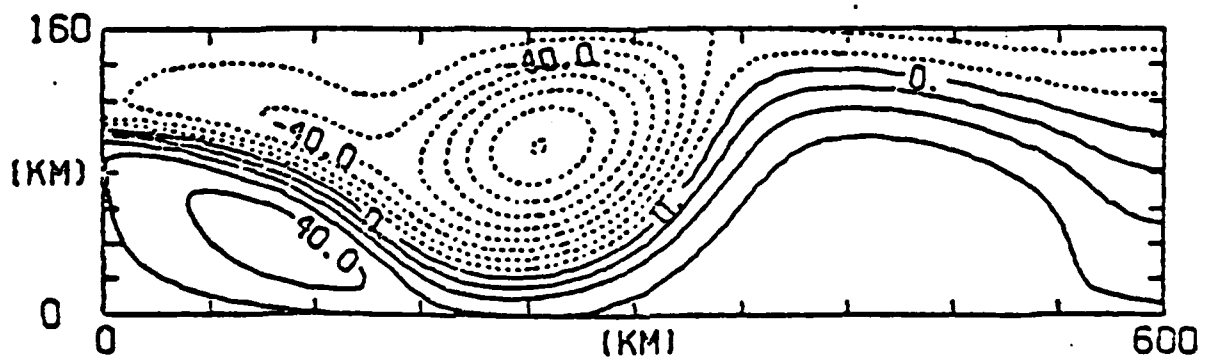

Figure 9b. Semi-implicit reduced gravity model solution with due east inflow.

A series of experiments was also made to test the effect of the island. Results show that if the jet entering the basin at an angle has too large a velocity (> 50 cm/sec), the island deflects the jet to its north (Figure 10) and the Alboran gyre disappears.

A number of experiments were also performed to test the effect of decreasing inflow. Figure 11 shows a time series of solutions which was initialized using the day 360 solution of the pivotal case. Velocity was then allowed to decrease to 1 cm/sec over a period of 180 days. Although the anticyclonic circulation always remains in the western part of the basin, it diminishes both in strength and horizontal dimensions. Also of note is the small cyclonic cirulation which moves westward and intensifies. This movement brings about the existence of two gyres west of Alboran Island, a rather unique situation sometimes observed in the satellite infrared imagery.

These results all point to the importance of knowing the magnitude of the incoming velocity as well as its direction. The Alboran gyre appears to be very sensitive to these changes. Thus in order to predict the characteristics of the gyre, a time series of the velocity entering the Strait of Gibraltar seems necessary.

Experiments using the explicit reduced gravity model have been recently initiated and used to test the effects of climatological wind stress. This test is designed to determine the circulation due solely to wind stress in the Alboran Sea. The second case is forced by 30 cm/sec inflow alone for 360 days and wind stress force is then added.

Figure 12a, b, c and d show solutions from the third year of integration at mid month for January, April, July and October. The conclusion may be drawn from these solutions, that climatological wind stress alone is responsible for a somewhat weak but consistent anticyclonic circulation in the western Alboran Sea. These monthly solutions also show that wind forcing results in small time variations in the circulation of the Alboran Sea. Figure 13 represents the basin averaged kinetic and potential energy for the three years of

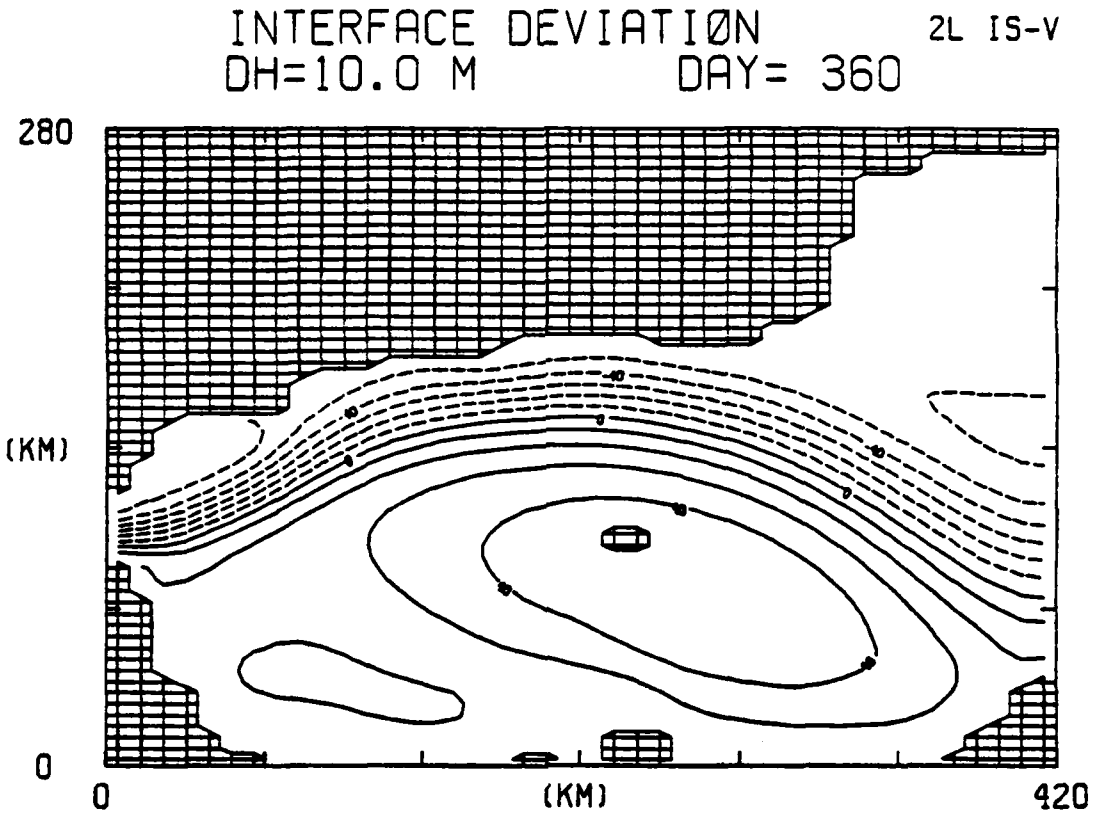

Figure 10. Two layer solution with 100 cm/sec incoming, angled velocity.

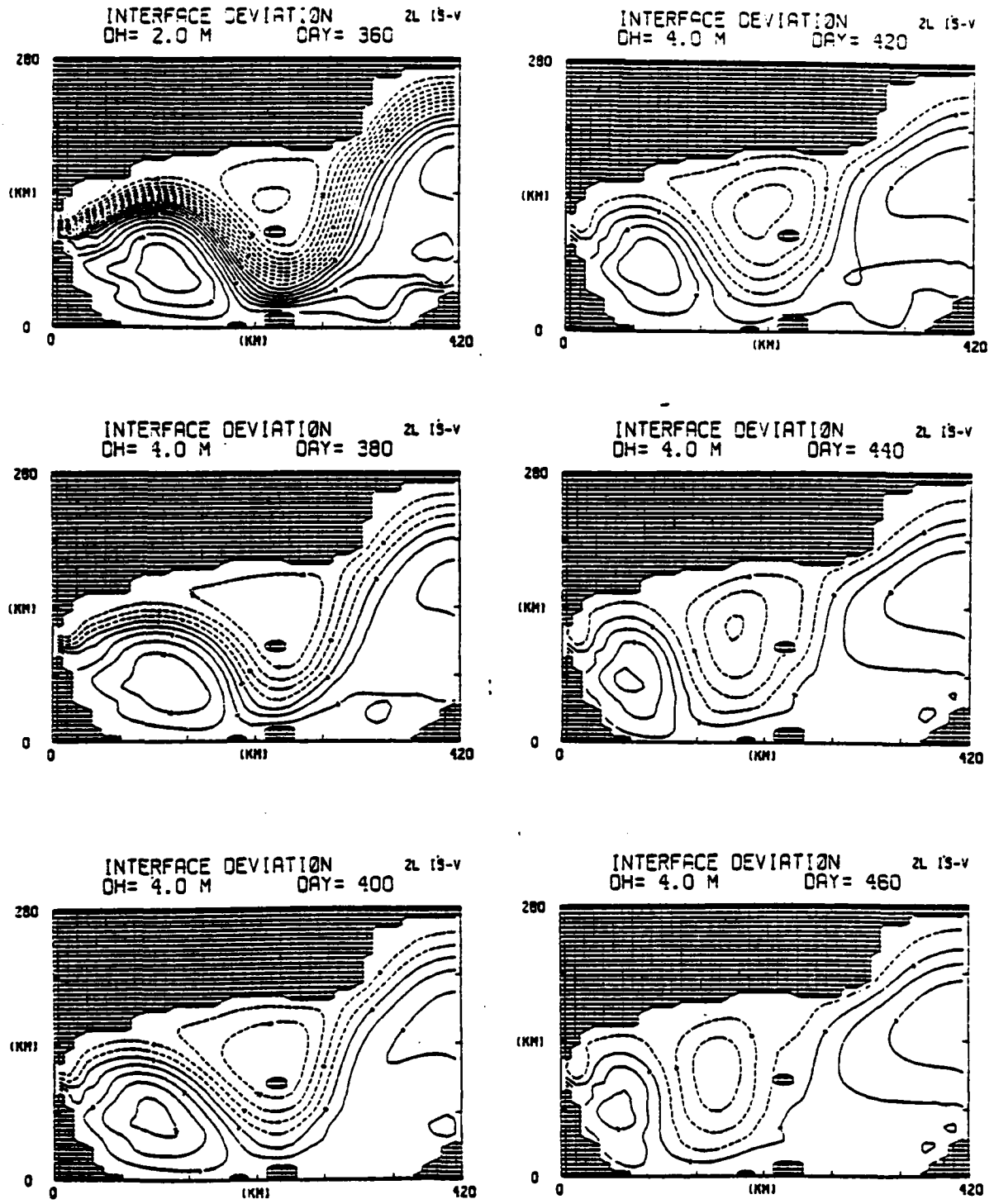

Figure 11. Two layer solutions of angled inflow decreasing from 30 cm/sec to 1 cm/sec over a period of 180 days.

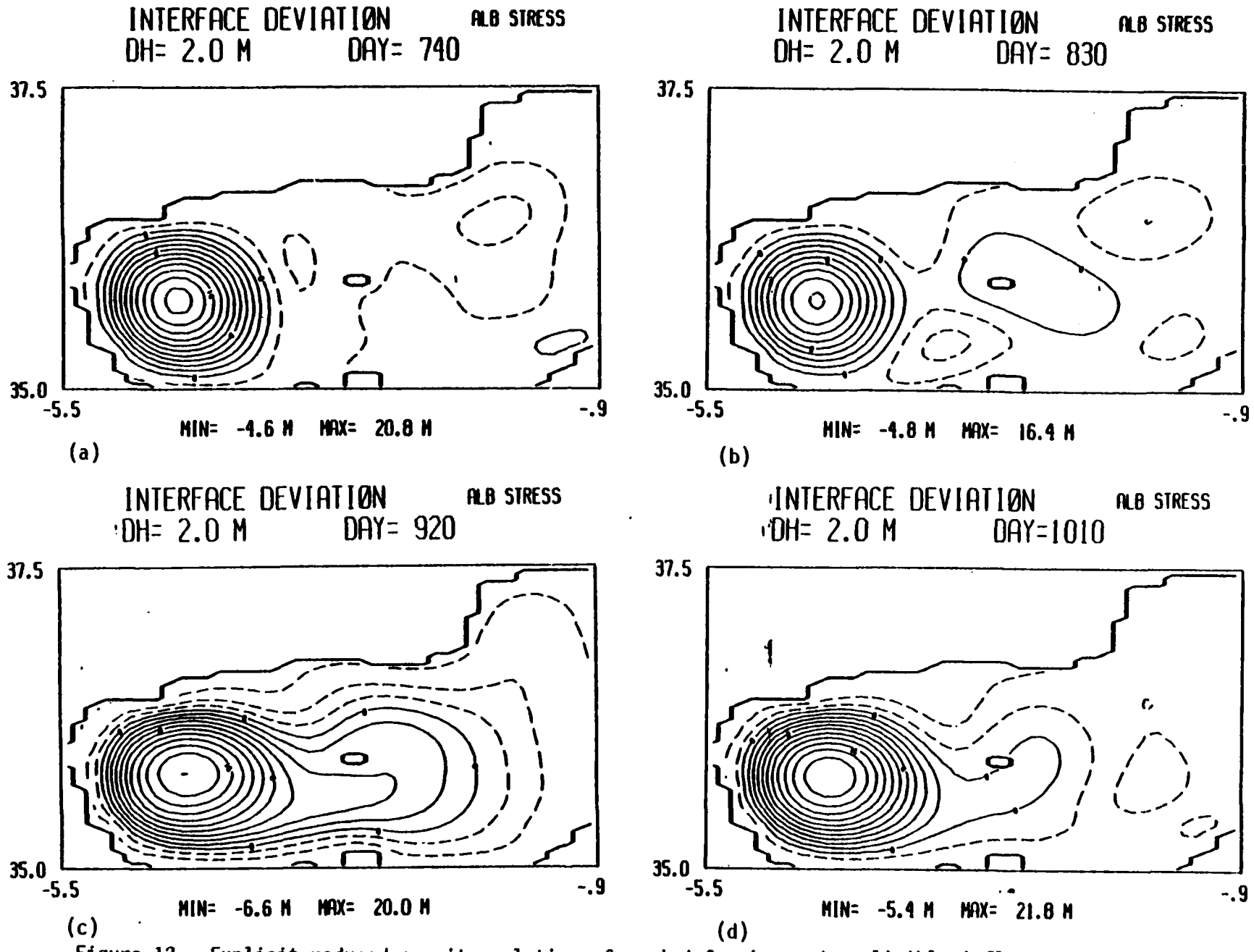

Figure 12. Explicit reduced gravity solutions for wind forcing and negligible inflow during (a) January, (b) April, (c) July and (d) October of the third year.

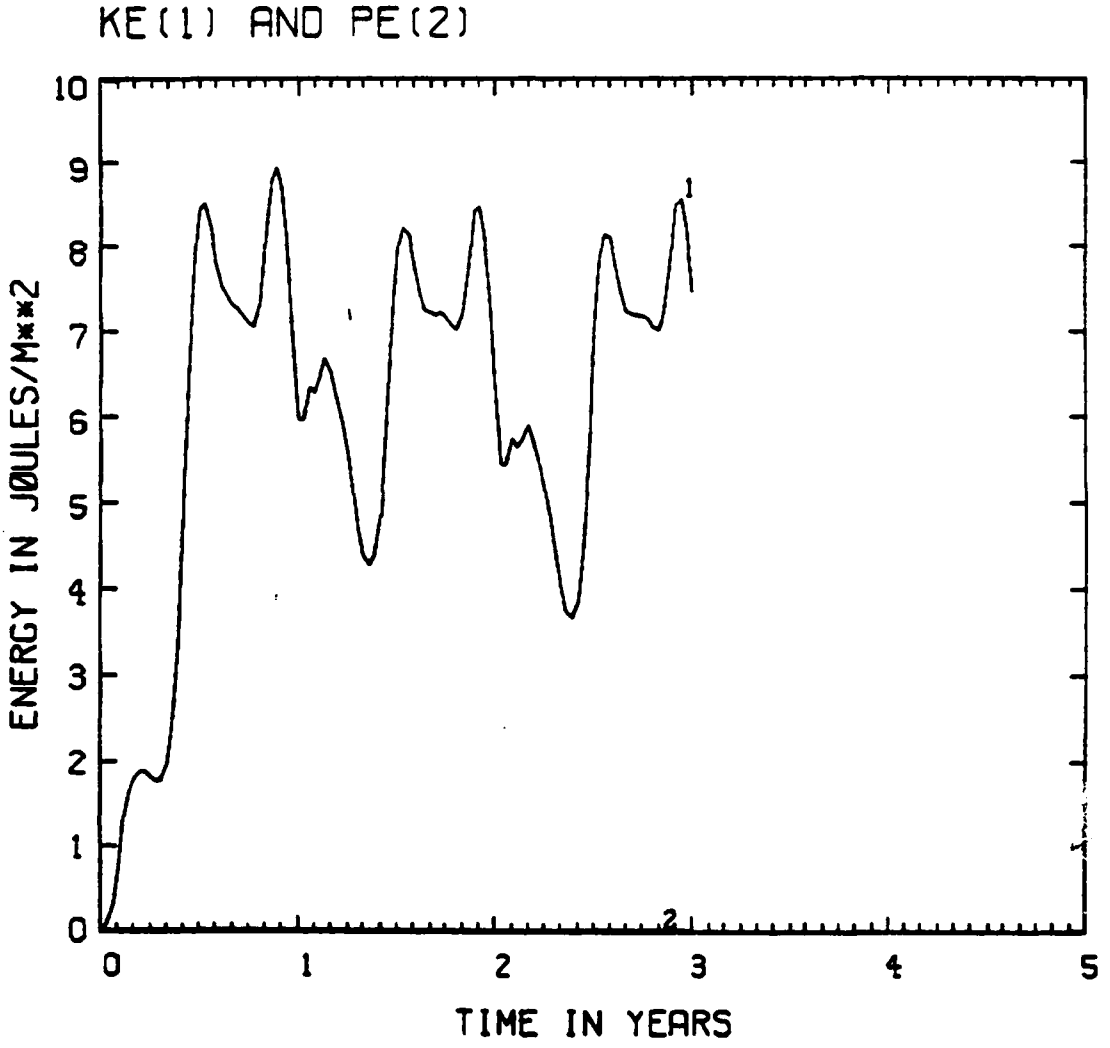

MAX= 3.5E 02. MIN=-8.5E-02. IC= 3.5E 00

Figure 13. Basin averaged kinetic and potential energy for the three years of the wind driven case.

integration. These curves show that although energy varies during the year, a yearly pattern develops and repeats, indicating that a steady state has been reached.

Figure 14 presents the solution of the second experiment after 350 days of integration using 30 cm/sec inflow. At day 360, the climatological wind forcing was added and the model was integrated for three more years. Results from January, April, July and October of the fourth year are presented in Figure 15a, b, c and d. The addition of the wind enhances the horizontal dimensions and intensity of the gyre. These solutions also show small scale changes in the circulation with time due to the wind stress. Figure 16 shows the basin averaged energy curves for the four years of this experiment. Solutions appear to approach a steady state by year four. Thus from a climatological point of view wind stress assists the development of an anticyclonic gyre throughout the year.

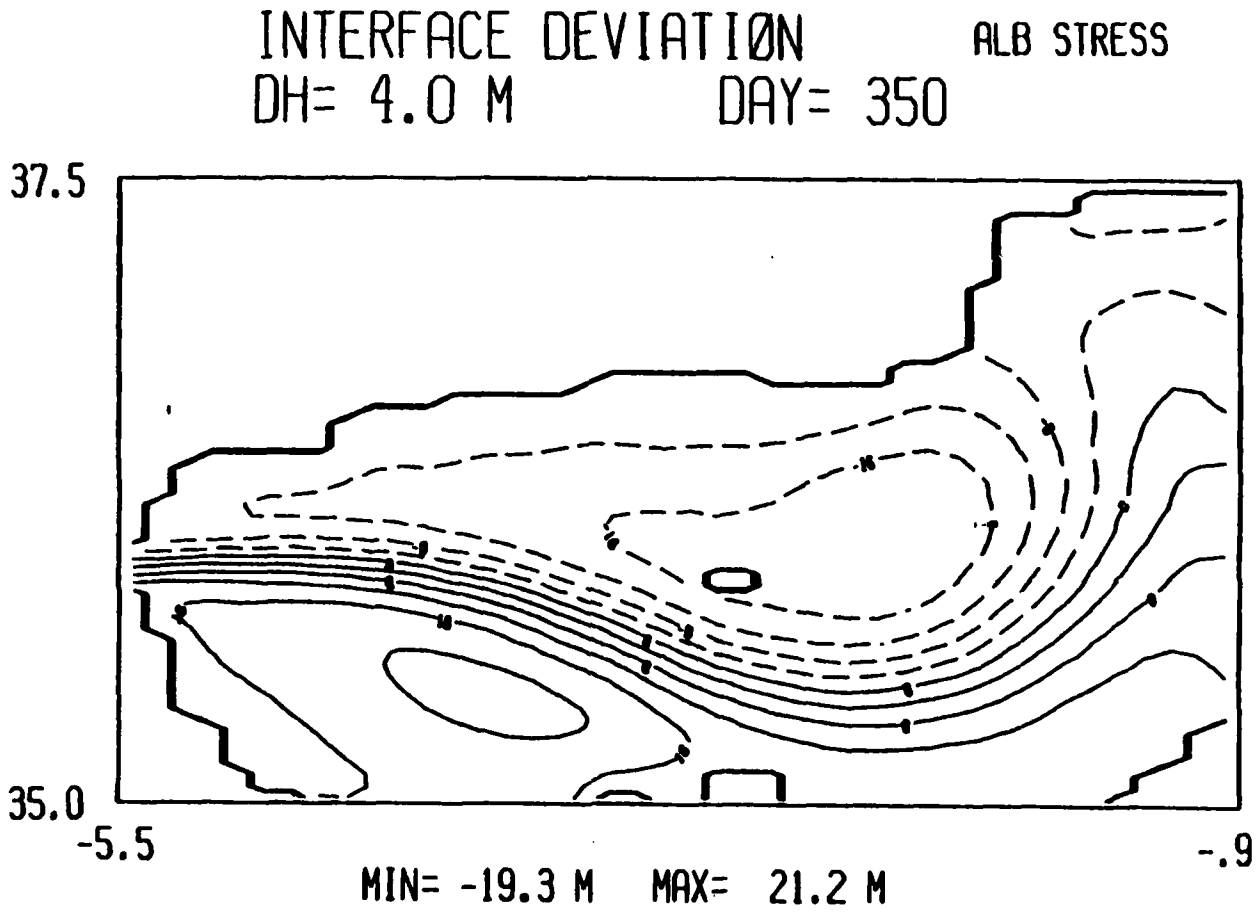

Figure 14. Solution of the port driven (30 cm/sec) only, explicit reduced gravity case.

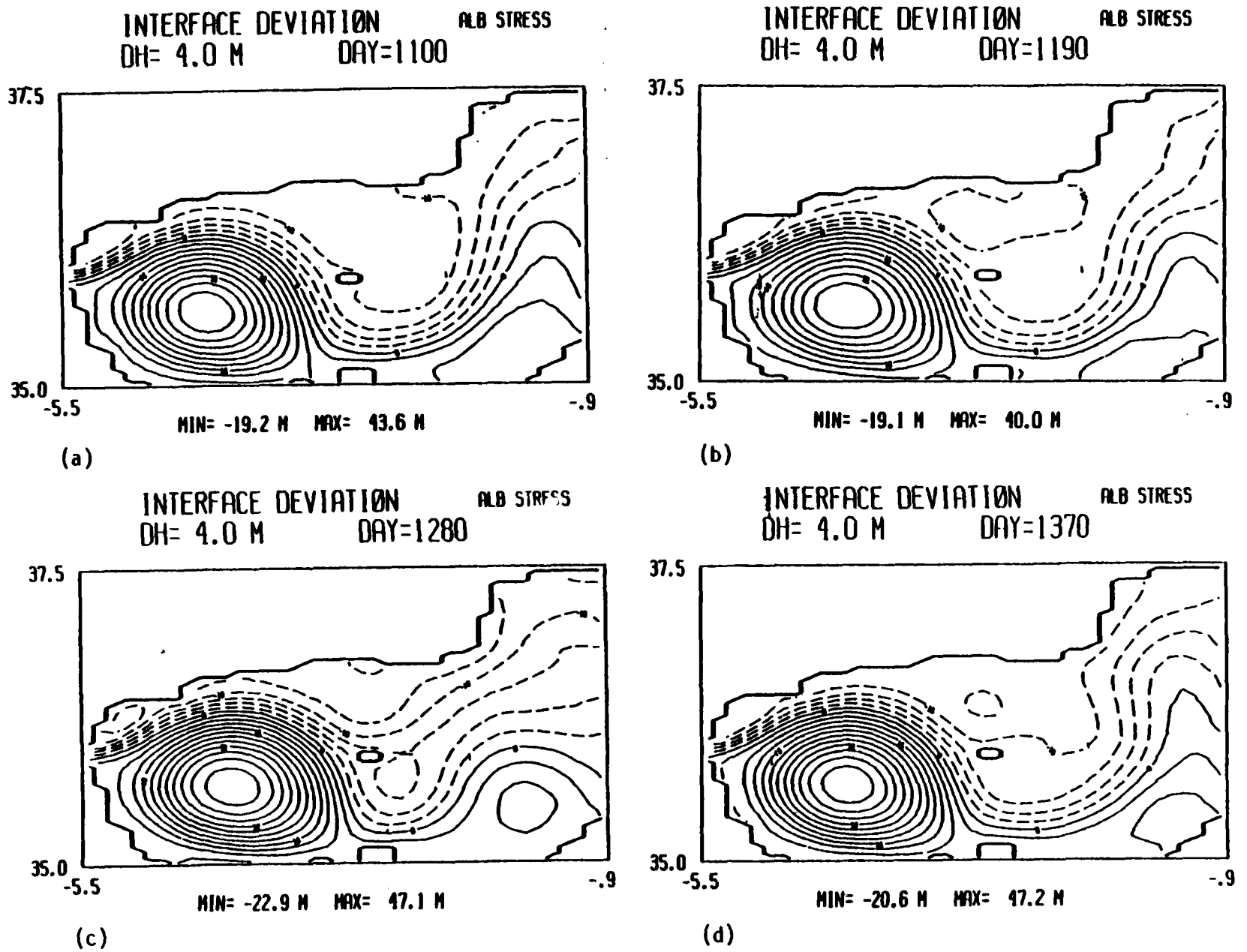

Figure 15. Solutions of the wind and port driven explicit reduced gravity case for (a) January, (b) April, (c) July and (d) October of the fourth year.

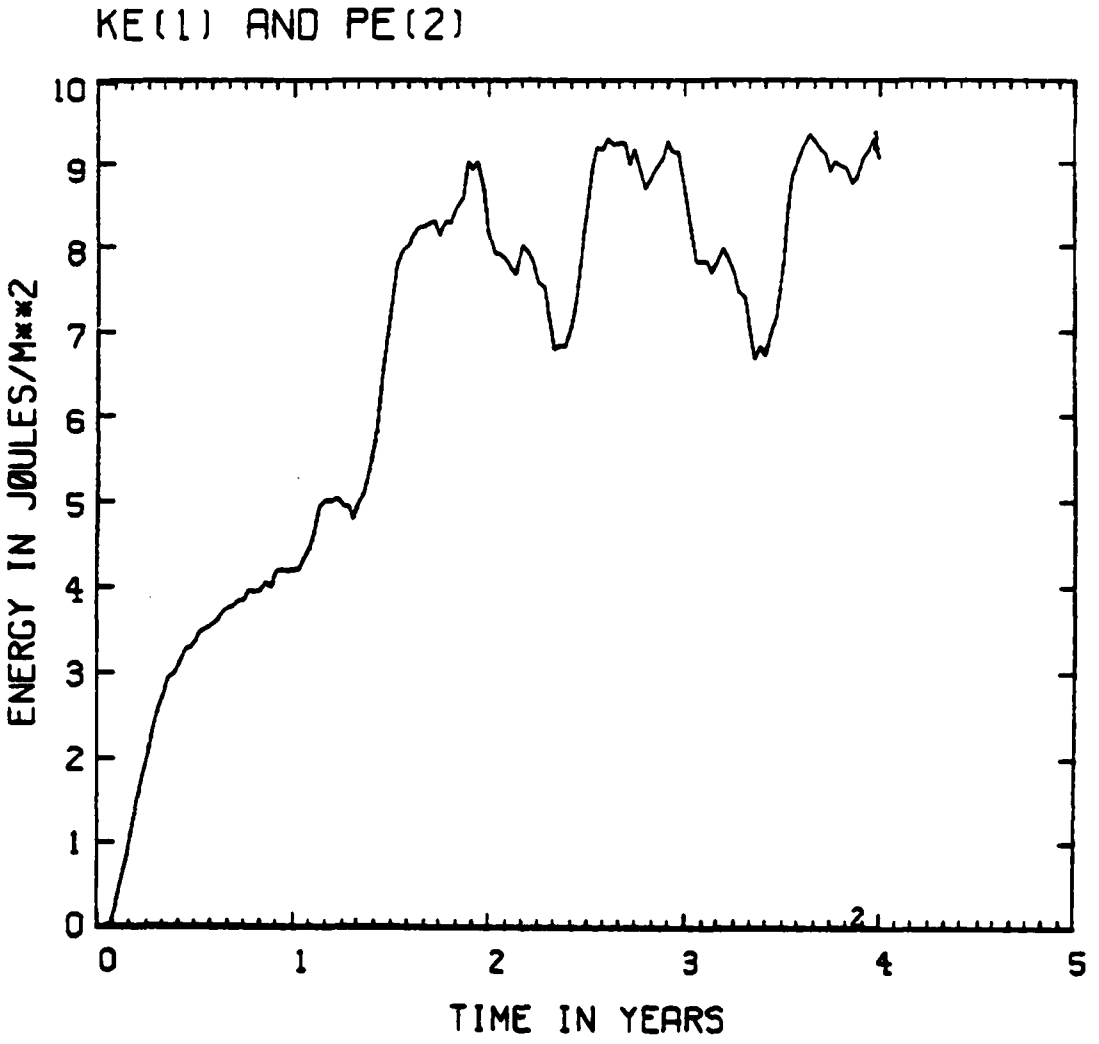

MAX= 1.5E 03. MIN=-2.0E-01. IC= 1.5E 01

Figure 16. Basin averaged kinetic and potential energy for the four years of the port and wind driven case.

SUMMARY

The non-linear reduced gravity and two layer models of Hurlburt and Thompson (1980) have been adapted (Preller and Heburn, 1983) to study circulation in the Alboran Sea. Model results using real geometry and topography in a two layer model show little effect upon the upper layer by the slowly moving lower layer. More important are the effects of a coastal feature Cape Tres Forcas, which deflects the flow from the southern boundary. Also, the Alboran Island deflects the incoming jet to its north if velocities greater than 50 cm/sec are used at inflow. Additional experiments show the high sensitivity of the Alboran gyre to changes in the magnitudes of the inflow, indicating that a thorough knowledge of the inflow magnitude, direction and time variation is necessary to predict the characteristics of the gyre. Reduced gravity solutions forced by monthly mean climatological wind stress shows that climatological wind stress enhances the gyre throughout the year and causes some small time varying changes in the circulation of the entire basin.

REFERENCES

Bethoux, J. P., 1979. Budgets of the Mediterranean Sea. Their dependence on the local climate and on characteristic of the Atlantic waters. Oceanol. Acta. 2, 2: 137-163.

Burkov, V. A., Drivosheya, V. G. Ovchinnikov, I. M. and Savin, M. T., 1979. Eddies in the current system of the western Mediterranean Basin. Oceanology, 19: 9-13.

Cheney, R. E., 1977. Recent observations of the Alboran Sea front. NAVOCEANO Technical Note 370073-77, 24 pp.

Cheney, R. E., 1978. Recent observations of the Alboran Sea frontal system. J. Geophys. Res., 83: 4593-4597.

Gallagher, J. J., Fecher, M. and Gorman, J., 1981. Project HUELVA oceanographic/acoustic investigation of the western Alboran Sea. NUSC Technical Report 6023, 106 pp.

Grousson, R. and Faroux, J. 1963. Measure de courants de surface en Mer d'Alboran. Cah. Oceanogr., 15: 716-721.

Hurlburt, H. E. and Thompson, J. D., 1980. A numerical study of Loop Current intrusions and eddy shedding. J. Phys. Oceanogr., 10: 1611-1651.

Katz, E. J., 1972. The Levantine intermediate water between the Straight of Sicily and the Strait of Gibralter. Deep Sea Res., 19: 507-520.

Lacombe, H., 1961. Contribution A L'Etude du Regime du Detroit de Gibralter. Cah. Oceanogr., XIII: 74-107.

Lacombe, H., 1971. Le Detroit de Gibraltar. Note et Memoires de Service Geologique du Maroc., No 222 bis, 111-146.

Lacombe, H., 1982. Regime of the Strait of Gibraltar and of its east and west approaches. In: J. C. J. Nihoul (Editor), Hydrodymanics of semi-enclosed seas. Elsevier, Amsterdam, pp.

Lanoix, F., 1974. Project Alboran Etude Hydrologique Dynamique de la Mer d'Alboran. Tech. report 66, N. Atl. Treaty Org. Bussels, pp 39.

May, P.W., 1982. Climatological flux estimates in the Mediterranean Sea: Part I. Winds and wind stress. Naval Ocean Research and Development Activity, NSTL Station, MS. NORDA Technical Report 54, p. 56.

Mommsen, D. B., Jr., 1978. The effect of wind on sea surface temperature gradients in the Strait of Gibraltar and Alboran Sea. Report from Fleet Weather Central, Rota, Spain, 18 pp.

Nof, D., 1978. On geostrophic adjustment in Sea straits and estuaries: theory and laboratory experiments. Part II. Two-layer system J. Phys. Oceanogr., 8: 861-872.

Ovchinnikov, I. M., 1966. Circulation in the surface and intermediate layers of the Mediterranean. Oceanology, 6: 48-59.

Ovchinnikov, I. M., Krivosheya, V. G. and Maskalenko, L. V., 1976. Anamalous features of the water circulation of the Alboran Sea during the summer of 1962. Oceanology, 15: 31-35.

Peluchon, G. and Donguy, J. R., 1962. Travauz Oceanographiques d "l'Origny" dans le Detroit de Gibraltar. Compaigne internationale - 15 mpi, 15 Juin 1961. Zemi partie. Hydrologie en Mer d'Alboran. Cah. Oceanogr., 14: 573-578.

Petit, M., Klaus, V. Gelci, R., Fusey, F., Thery, J. J. and Bouly, P., 1978. Etude d'un tourbillon oceanique d'echelle moyenne en mer d'Alboran par emploi conjoint techniques spatiales et oceangraphiques. C. R. Acad. Sci. 287: 215-218.

Porter, D. L., 1976. The anticyclonic gyre of the Alboran Sea, Independent research report from M.I.T.-WHOI joint program, Woods Hole, Ma, pp 29.

Stevenson, R. W., 1977. Huelva Front and Malaga, Spain eddy chains as defined by satellite and oceanographic data. Deut. Hydrogr. A. 30, 2: 51-53.

Stommel, H., Bryder, H. and Magelsdorf, p., 1973. Does some of the Mediterranean outflow come from great depth? Pure and Appl Geophysics. 105: 879-889.

Wannamaker, B., 1979. the Alboran Sea Gyre: Ship satellite and historical data SCALANT ASW Research Centre Report Sr-30, La Spezia, Italy, 27 pp.

Preller, R. and H. E. Hurlburt, 1982. A Reduced gravity numerical model of circulation in the Alboran Sea. In: J.C.J. Nihoul (Editor) Hydrodynamics of semi-enclosed seas. Elsevier, Amsterdam, 75-89.

Preller, R. H. and G. W. Heburn, 1983. A simple numerical model of circulation in the western Mediterranean Sea submitted to Oceanoligica Acta.

Vanwyckhouse, R. J., 1973. Synthetic Bathymetric Profiling System (SYNBAPS). Naval Oceanographic Office, Washington, DC Technical Report 233, p. 138.

Vanwyckhouse, R. J., 1979. SYNBAPS, Volume I - Data sources and data preparation. Naval Ocean Research and Development Activity, NSTL Station, Ms, NORDA Technical Note 35.

VERTICAL SHEAR FROM TOPS

INTRODUCTION

The growth and propagation of internal waves in the world oceans is often attributed to the regions of strong gradients in velocity (vertical shear) and density. To predict the spatial and temporal distribution of density and velocity gradients would require an extensive effort in ocean surveys modeling.

Numerous field experiments have used high resolution velocity and velocity/temperature microstructure profilers to measure vertical variation of shear, temperature, Richardson number and turbulence disspation. For a review of these experiments see Harding et al., 1983. Though these experiments were performed at various regions in the northern hemisphere, most were performed over relatively short time scales (a few days). Thus it would be a practical impossibility to measure or predict from experimental data sources alone, the density and velocity gradients over large time and horizontal space scales. Numerical forecasting of these upper ocean properties with verification by properly designed field programs serves as a useful alternate approach.

The best candidate for such a modeling effort is the Thermodynamic Ocean Prediction System (TOPS) currently operational at Fleet Numerical Ocean Center (FNOC) (Clancy and Martin, 1981). This model provides the upper ocean currents required to synoptically forecast upper ocean vertical shear over large regions of the world's ocean. TOPS additionally provides velocity components through the mixed layer making it potentially useful for shear forcasting.

MODELING APPROACH

The TOPS model is basically a Level II turbulence closure model of Mellor and Yamada (1974). The model results in an isopycnal mixed layer with vertical uniformity due to mixing caused by wind induced shear instability and surface cooling. During strong wind forcing and/or strong surface cooling, the mixed layer deepens due to entrainment from below caused by turbulent mixing. During weak wind forcing and/or strong surface heating, the turbulent energy decreases to the point where active entrainment at the base of the mixed layer is no longer maintained and the layer shallows. This model has been extensively tested against observations by Warn-Varnas, Dawson (1981) and Martin (1982, 1983) at specific experimental and weather ship locations. It has also been tested in the operational sense by Clancy and Martin (1979), Clancy et al., (1981), and Clancy and Pollak (1982).

Forcing for the TOPS model is derived from the Navy's global weather prediction model NOGAPS in the form of surface stresses and heat fluxes. It is initialized and updated by an analysis scheme which uses the TOPS forecast products for first guess fields and blends them with daily XBT observations and satellite derived SST fields. The TOPS model is essentially a 3-D mixed layer model consisting of a grid of profiles, but with advection of temperature and salinity between grid points. At FNOC, TOPS runs on the standard 63 x 63 northern Hemispheric polar stereographic grid with 381 km grid resolution at 60 N, Figure 17. The vertical grid has irregularly spaced levels with Δz varying from 5 km at the surface to 100 km below the 200 m level (Figure 18). Bottom boundary conditions specify constant values of temperature, salinity and velocity; surface boundary conditions specify fluxes of heat, precipitation or evaporation and momentum. Lateral boundary conditions specify no inflow or outflow and zero fluxes of heat and salinity.

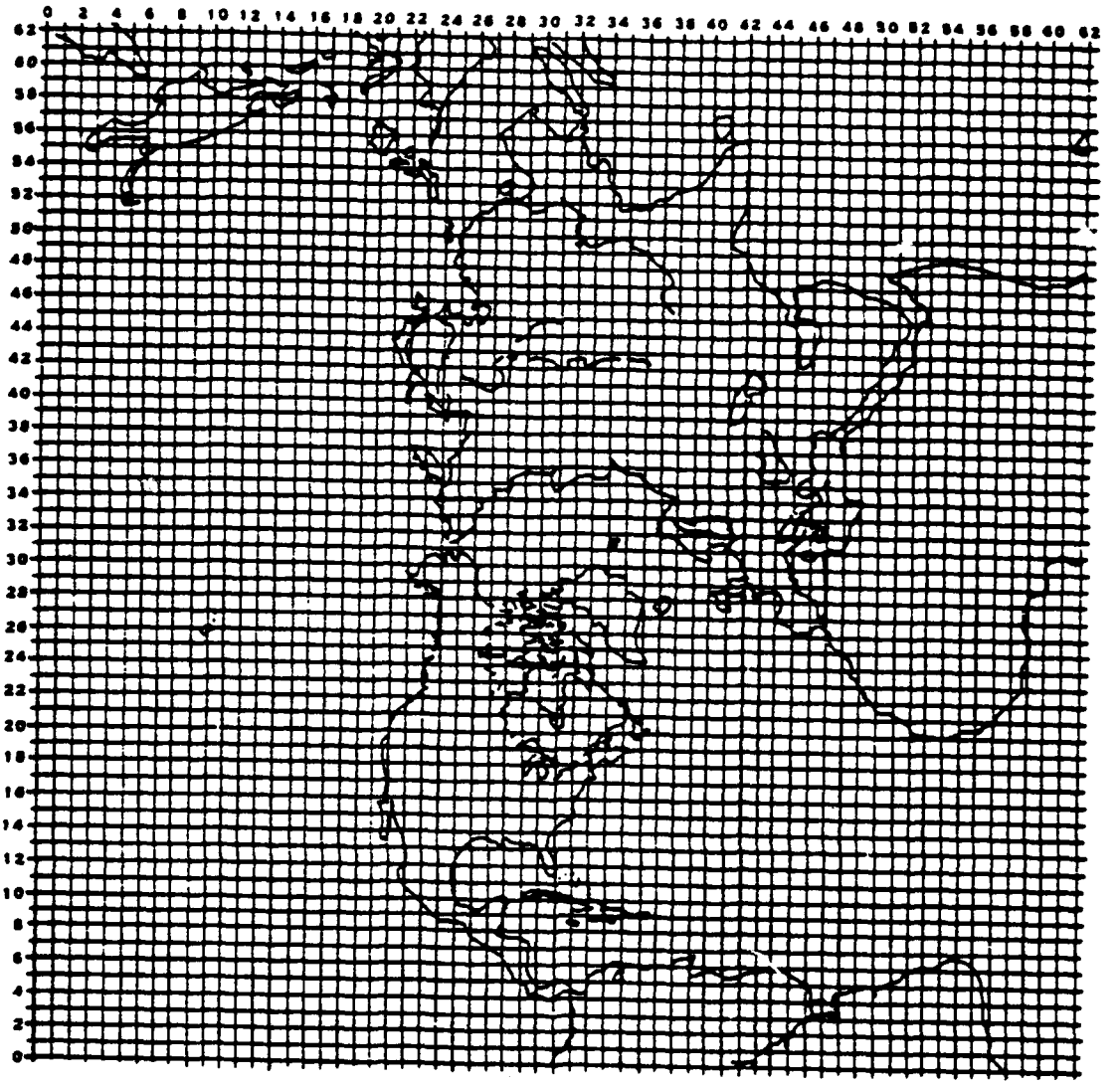

Figure 17. Standard 63 x 63 Northern Hemisphere Polar Stereographic Grid on which T, S, u, v and w_a are defined.

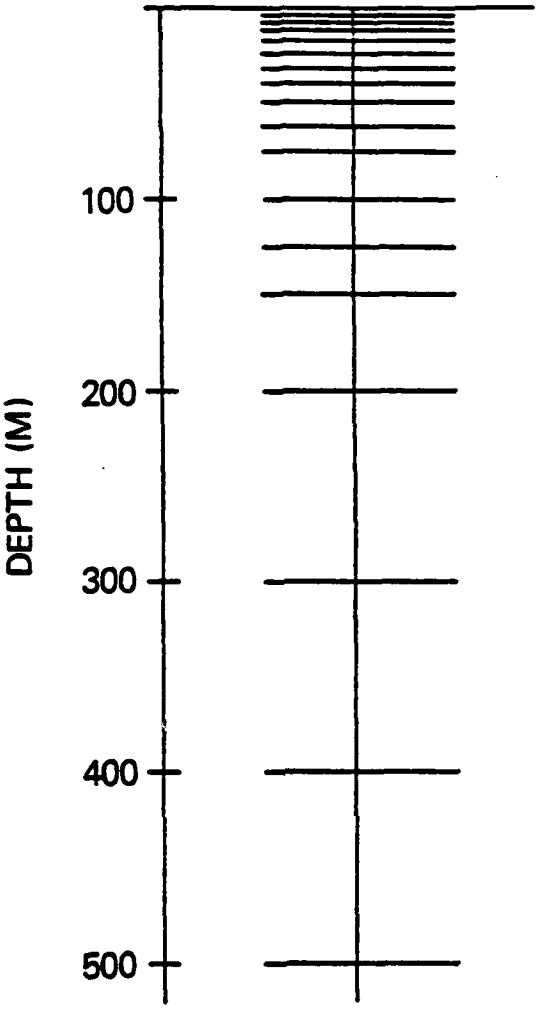

Figure 18. Vertical grid utilized by TOPS. The quantities T, S, u, v, u_a and v_a are defined at the depths indicated in the figure. All turbulence quantities and w_a are defined at depths midway between those shown in the figure.

EXPERIMENTAL APPROACH

The purpose of this study was to continue the research initiated last year (Harding et al., 1983) to investigate the potential of TOPS for shear prediction and to look at temporal and spatial variability of the TOPS output. In particular, this study investigated long term shear variations as well as seasonal comparisons.

At the time of these experiments, velocity fields from TOPS had not been archived for a long enough period of time to examine long term variations. Thus the version of TOPS which resides on the Texas Instrument Advanced Scientific Computer (TIASC) at the Naval Research Laboratory (NRL) in Washington was run continuously in a hindcast mode for six months. This version of the model is described in detail by Warn-Varnas et al., (1983) who used it to predict large scale thermal anomalies in the North Pacific. The FNOC analysis and model outputs required to force TOPS are also available at NRL over the entire northern hemisphere for extended time periods.

The chosen area of study is 12 x 21 point subregion of the 63 x 63 FNOC grid over the North Pacific, Figure 19. The TOPS model was integrated over the six month period March 2 through August 29, 1981. The model is initialized with March climatological salinity and March 2 thermal structure. The model was then run for approximately six months using FNOC 6 hourly wind and heat flux fields. A detailed explanation of initial conditions, boundary conditions and forcing functions are found in Warn-Varnas et al., (1983). An experiment has been conducted to determine over what period of time the solutions are affected by spurious motions induced by initialization. This time period appears to be 15-20 days. Thus only solutions after a 15 day initialization period are considered. The FNOC Extended Ocean Thermal Structure (EOTS) product provided the thermal structure initialization fields required. Table 2 lists the forcing fields, their source and frequency.

From hourly TOPS output, scalar shears

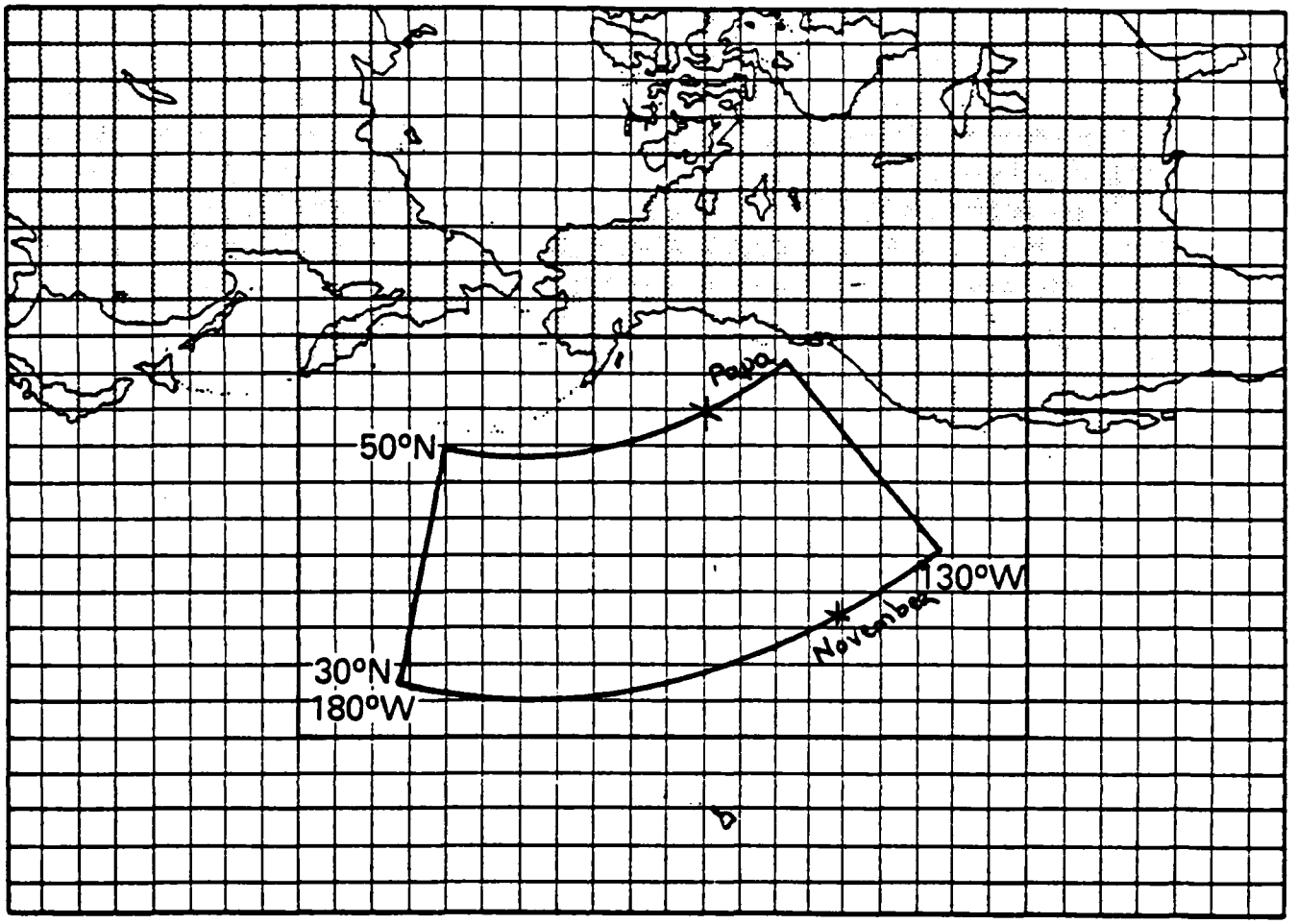

Figure 19. Subsection of the FNOC 63 x 63 Northern Hemispheric Polar stereographic Grid showing the domain (rectangle) and also includes latitudes 30-50 N and longitudes 180-130 W. Ocean Stations Papa and November are indicated on the grid.

$$S = ((du/dz)^2 + (dv/dz)^2)^{1/2}$$

were calculated at levels of TOPS located velocities. Z represents the vertical distance between the velocities given by the model. Also calculated, was the gradient Richardson number,

$$Ri = -(gd\rho/dz)/S^2$$

(ρ = water density at a given level, g = gravitation acceleration) at levels intermediate to the velocity levels. This number is a measure of the stability of the water column at that level. Yamada (1975), using a turbulence closure formulation similar to that used in TOPS, determined the critical flux of Richardson number exists between .18 - .27. Values above .25 indicate stability in the water column. Thus for this study values between 0. and .25 will be used to indicate shear instability.

TABLE 2
FNOC FIELDS USED FOR TOPS FORCING

FIELD	SOURCE	FREQUENCY
Boundary Layer Wind Speed	Planetary Boundary Layer Model	6 hourly
Boundary Layer Wind Direction	Planetary Boundary Layer Model	6 hourly
Solar radiation Flux	Primitive Equation Model	6 hourly
Total Heat Flux	Primitive Equation Model	6 hourly
Evaporative Heat Flux	Primitive Equation Model	6 hourly
Precipitation	Primitive Equation Model	12 hourly

TOPS model results will be presented in terms of contour plots and frequency distributions of shear and Richardson number for various levels and vertical cross sections within the North Pacific domain. The purpose is to investigate spacial and temporal variability of the potential FNOC shear product. The vertical cross sections of Richardson number show the dividing line between stable and unstable water, the pycnocline. Regions of shear instability are shaded in these figures. Note that in all plots depicting shear, values have been scaled upward by a factor of 10^4.

RESULTS

In previous studies (Harding et al., 1983), we examined the importance of short time scales, six hourly variations, diurnal variations and daily variations. These results showed a high degree of variability even on the shortest time scales. In this study, we will be concerned with seasonal time scales and long term trends in shear.

The first series of contoured plots will show monthly values of shear for the six months studied. Values are contoured for various levels and cross sections starting on March 17 and then depicted approximatley every 30 days.

Figure 20 shows lines of latitude and longitude along with land points over the North Pacific region studied. All level plots will be presented with this orientation. With reference to this horizontal orientation, cross sectional plots are made along lines drawn from the center point at the left boundary (6 of 12) and the center point of the top boundary (12 of 24).

Figure 21 shows a monthly time series of shear at level 2 (7.5 m). Most noticeable in this series of figures is the fact that the shear intensifies from March to August. The upper left corner of these plots develops into a region of consistently high shear (200×10^{-4}). Geographically, this region is to the south-southwest of the Bering Sea. It is a region of frequent intense storm and frontal passage. Harding et al., 1983, have shown that shear instability appears directly correlated to such frontal passage.

Figures 22 and 23 are histograms of the shear at level 2 (7.5 m) for the corresponding times. These figures clearly show the increase in magnitude of shear with time. Initially the average shear value centers around 8×10^{-3}. By summer, the average value is 1.4×10^{-2} with much higher values appearing then in spring.

The same times series for the long (left to right) cross section is shown in Figure 24. This time series shows the same trend as in the level series, larger magnitude shear developing in the summer.

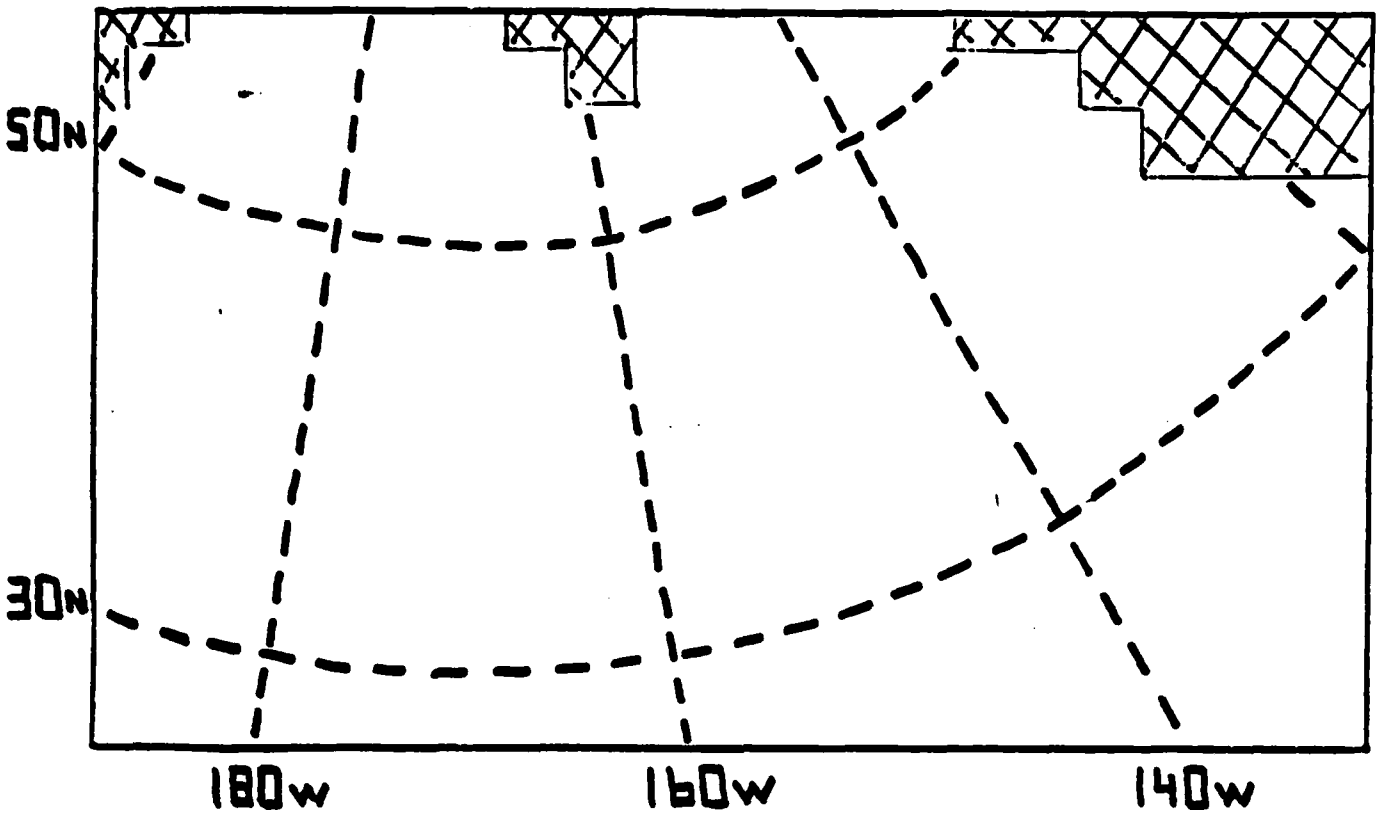

Figure 20. Model experimental subsection of the FNOC grid with land masked and latitude and longitude overlaid.

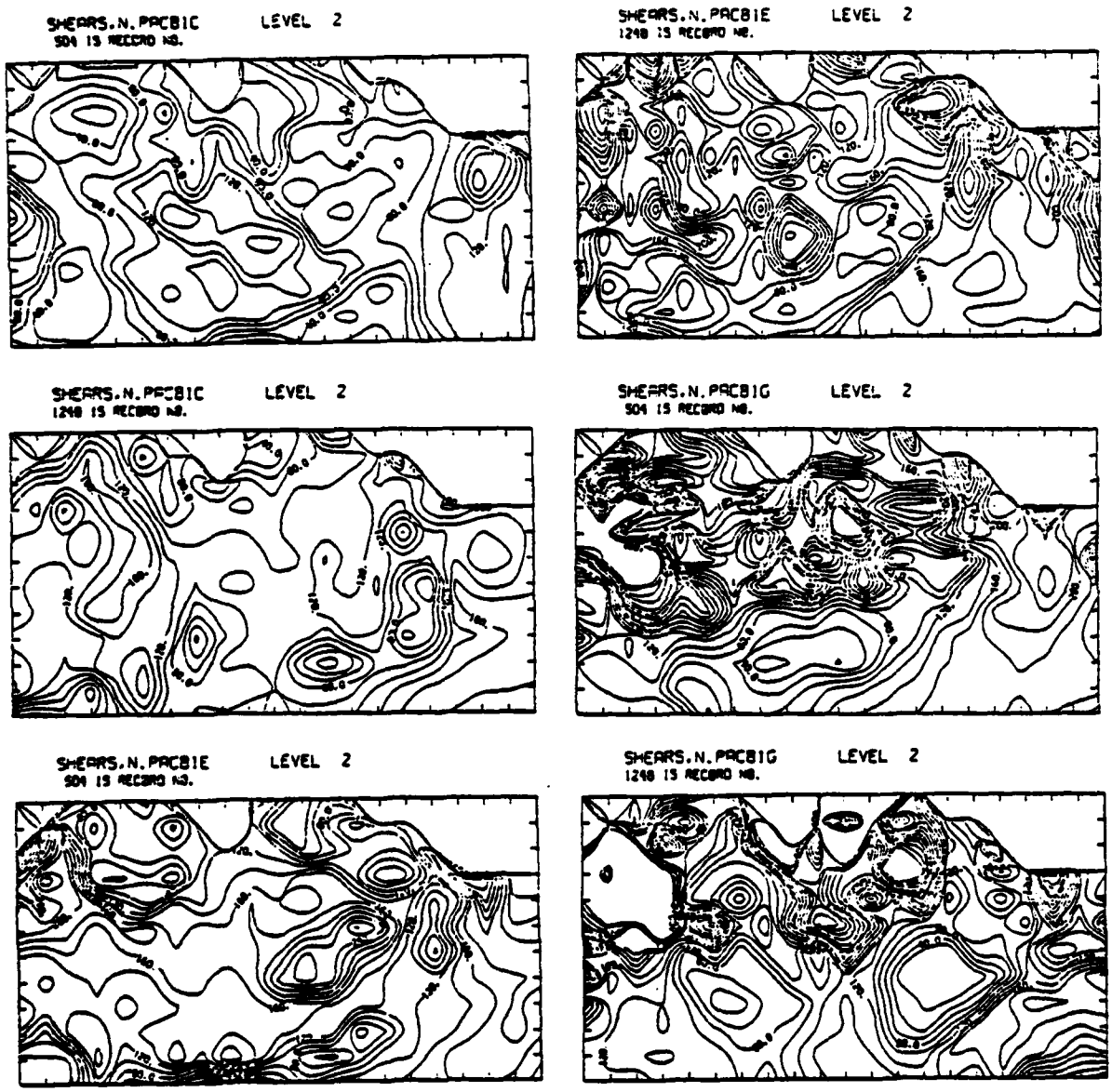

Figure 21. Monthly variation of the 7.5 m shear (s^{-1} x 10^4) for the months March through August.

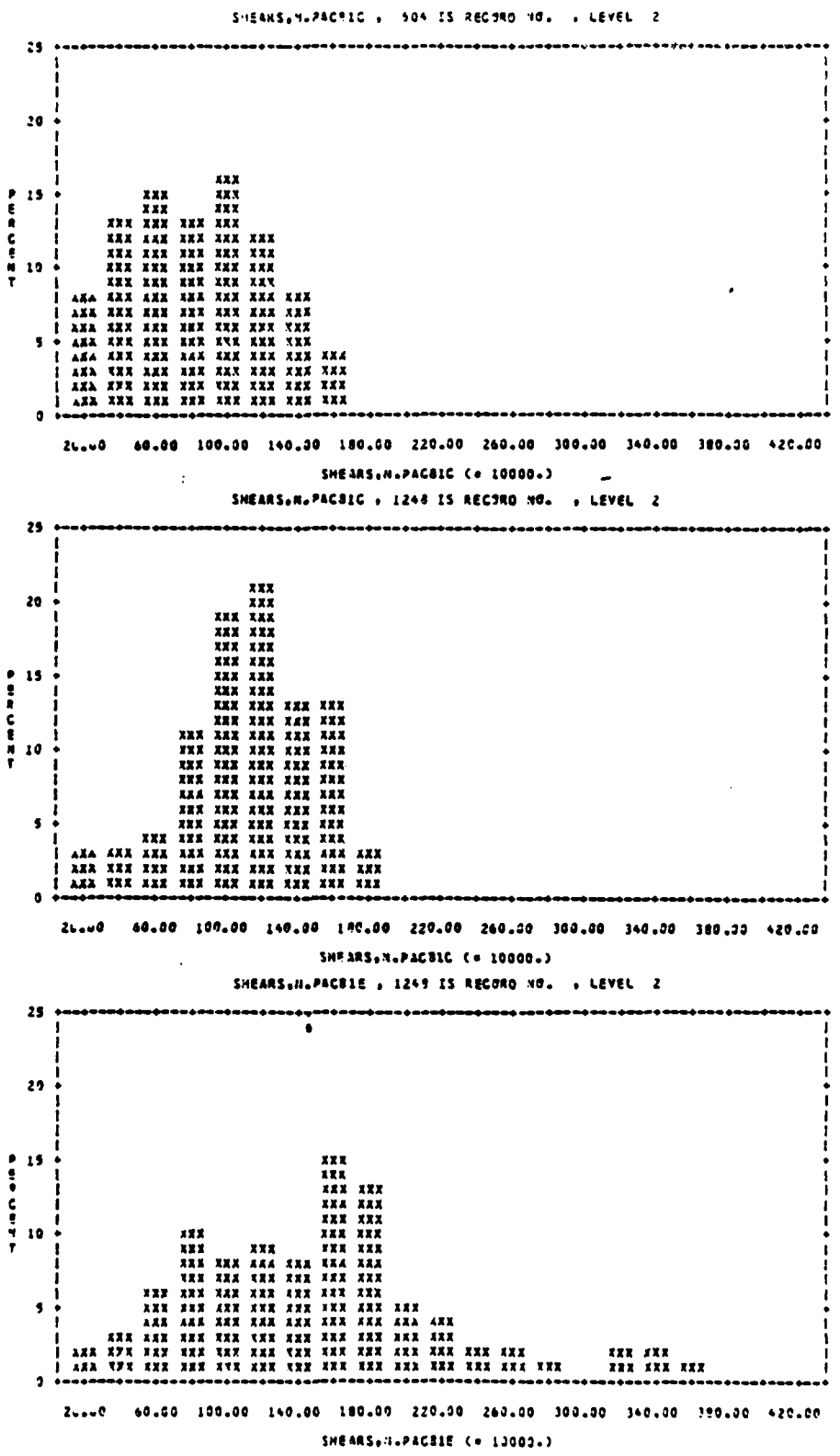

Figure 22. Frequency distribution of the 7.5 m shear (s^{-1} x 10^4) for the months March through May.

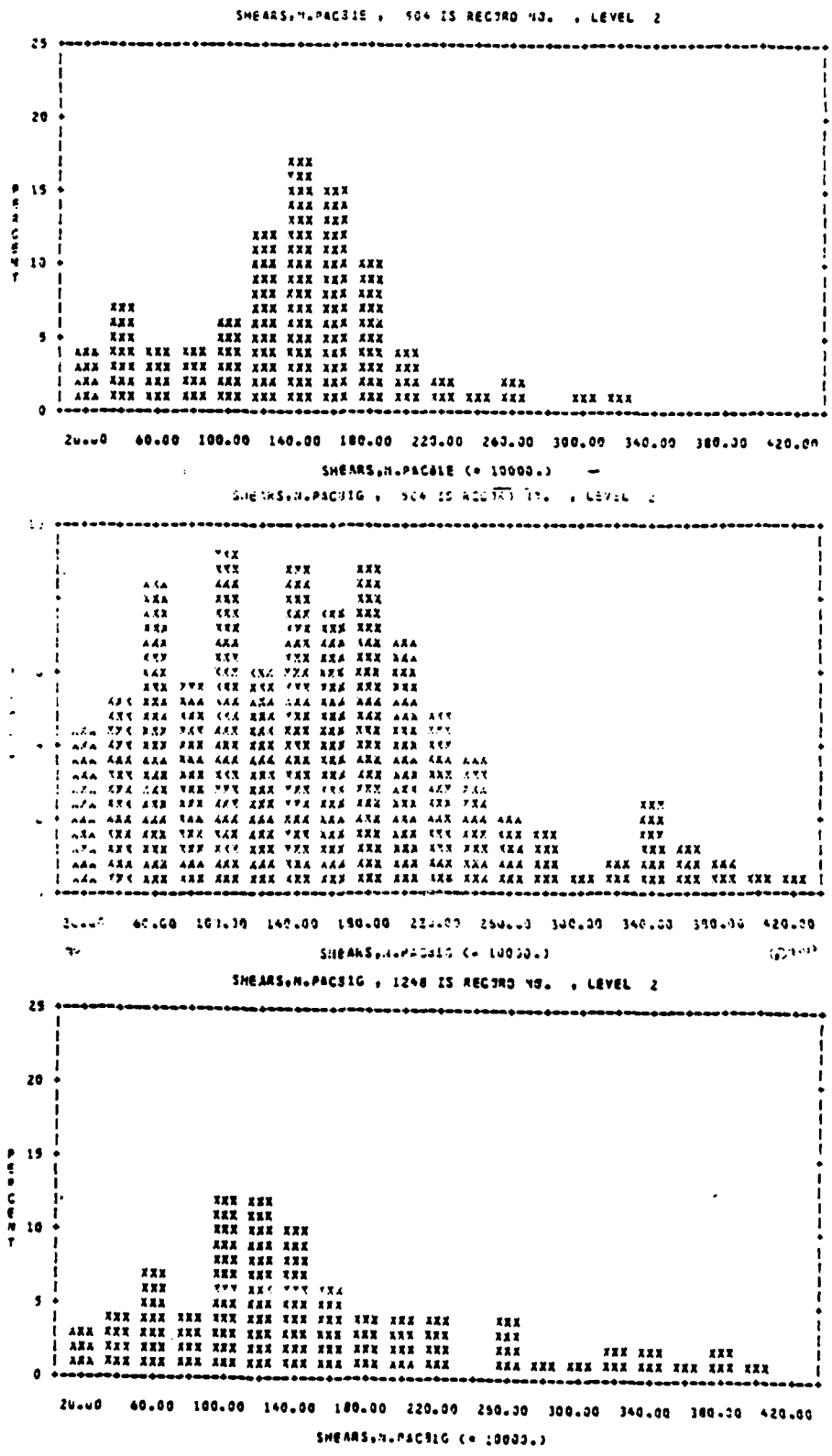

Figure 23. Frequency distribution of the 7.5 m shear (s^{-1} x 10^4) for the months June through August.

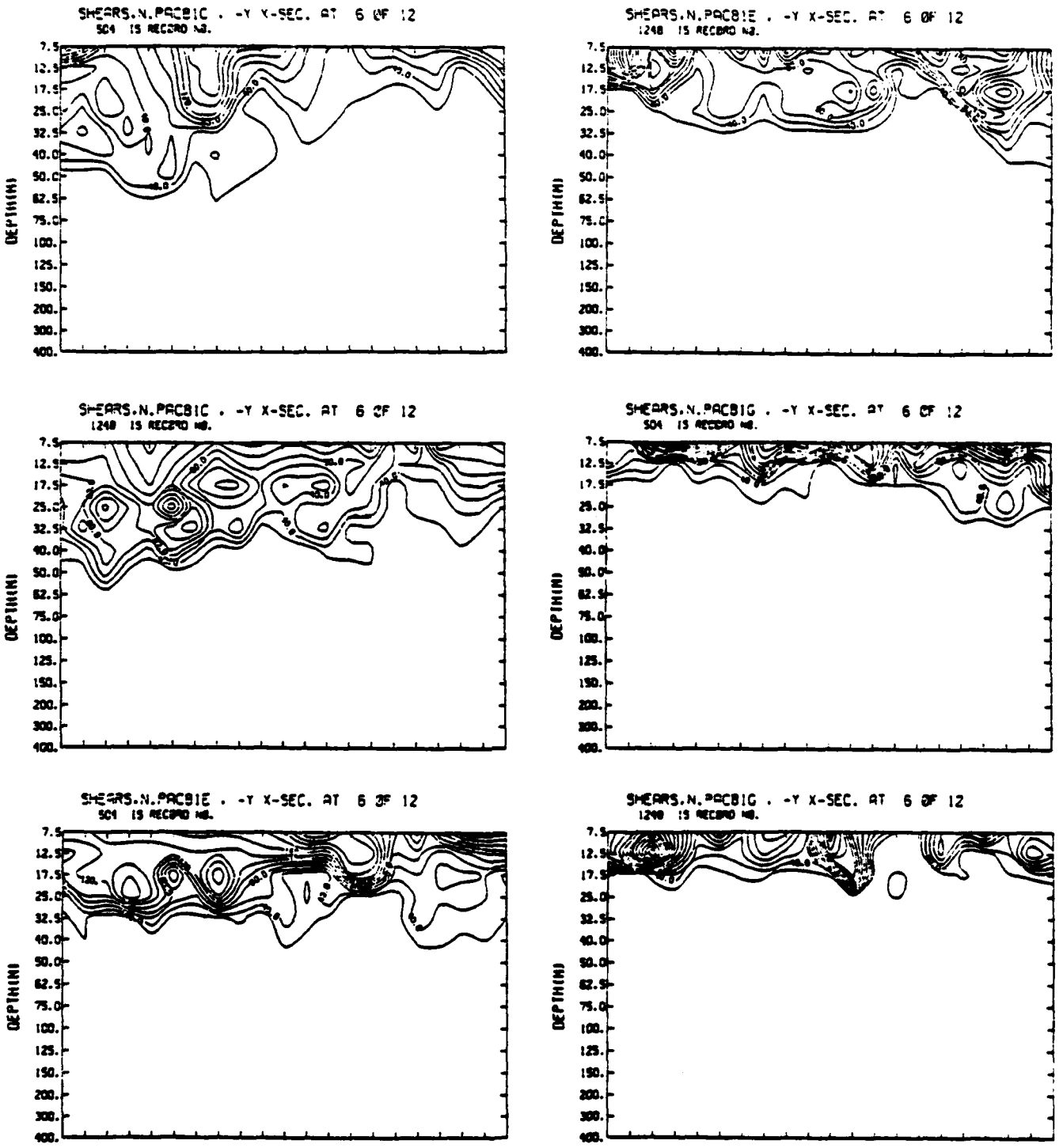

Figure 24. "Long" monthly cross sections of shear (s^{-1} x 10^4) for March through August.

However, it shows one more very important trend. If spring is defined as March-April with May-June as the transition period into summer, July-August, it becomes clear that shear extends to much greater depth in spring then in summer. The deepest shear lies in the region south of the Bering Sea, the same trend which was observed in the horizontal sections. The shallowing tendency is also apparent in the shorter cross sections, Figure 25. Again shear intensifies at the surface in the summer but extends to much greater depths in spring. Figures 26 and 27 are histograms of shear at level six. These figures also show the dramatic decrease in shear from spring to summer at 32.5 m depth. (Note the difference in scale on the y-axis when comparing). This existence of shear at depth in late winter - early spring is not an unexpected phenomenon. Figure 19 shows the location of Ocean Station Papa and Ocean Station November while Figures 28 and 29 show values of mixed layer depth during 1961 obtained from these stations. The maximum mixed layer depth exists in March and slowly decreases until there is a dramatic shallowing in June, July and August. This well known spring transition of the mixed layer occurs abruptly in response to an extended period of weak winds and strong surface cooling. Figure 30 further demonstrates the decrease in shear at depth using horizontal sections of the model results at level 6 (32.5 m). Active shear exists at this depth in March and April, diminishing in May and all but disappearing into the summer months. This shallowing of the mixed layer also explains the increase in shear magnitude during the summer. The model formulation conserves momentum within the mixed layer, thus as the layer shallows, velocity as well as shear will increase within the narrow mixed layer.

Level 6 was chosen as an average depth at which shear might exist for the entire six month period. The maximum depth to which shear extends is shown clearly in the vertical cross sections. Figure 31 shows values of shear starting at noon of March 17 and then for forty-eight hour intervals until noon of March 23. Using a contour interval of 5, the maximum depth of these contours extend below 125 m. Figure 32

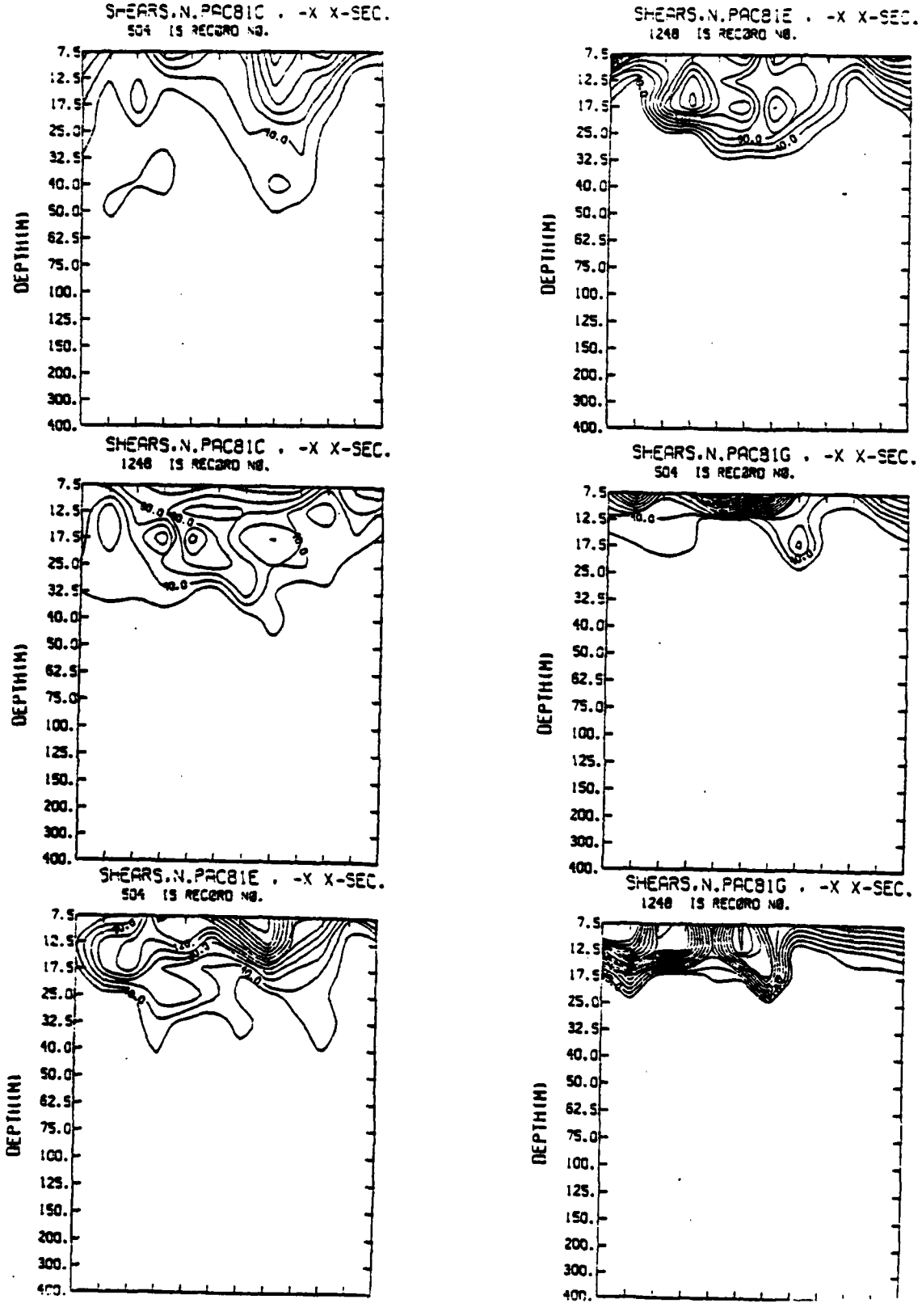

Figure 25. "Short" monthly cross sections of shear (s^{-1} x 10^4) for March through August.

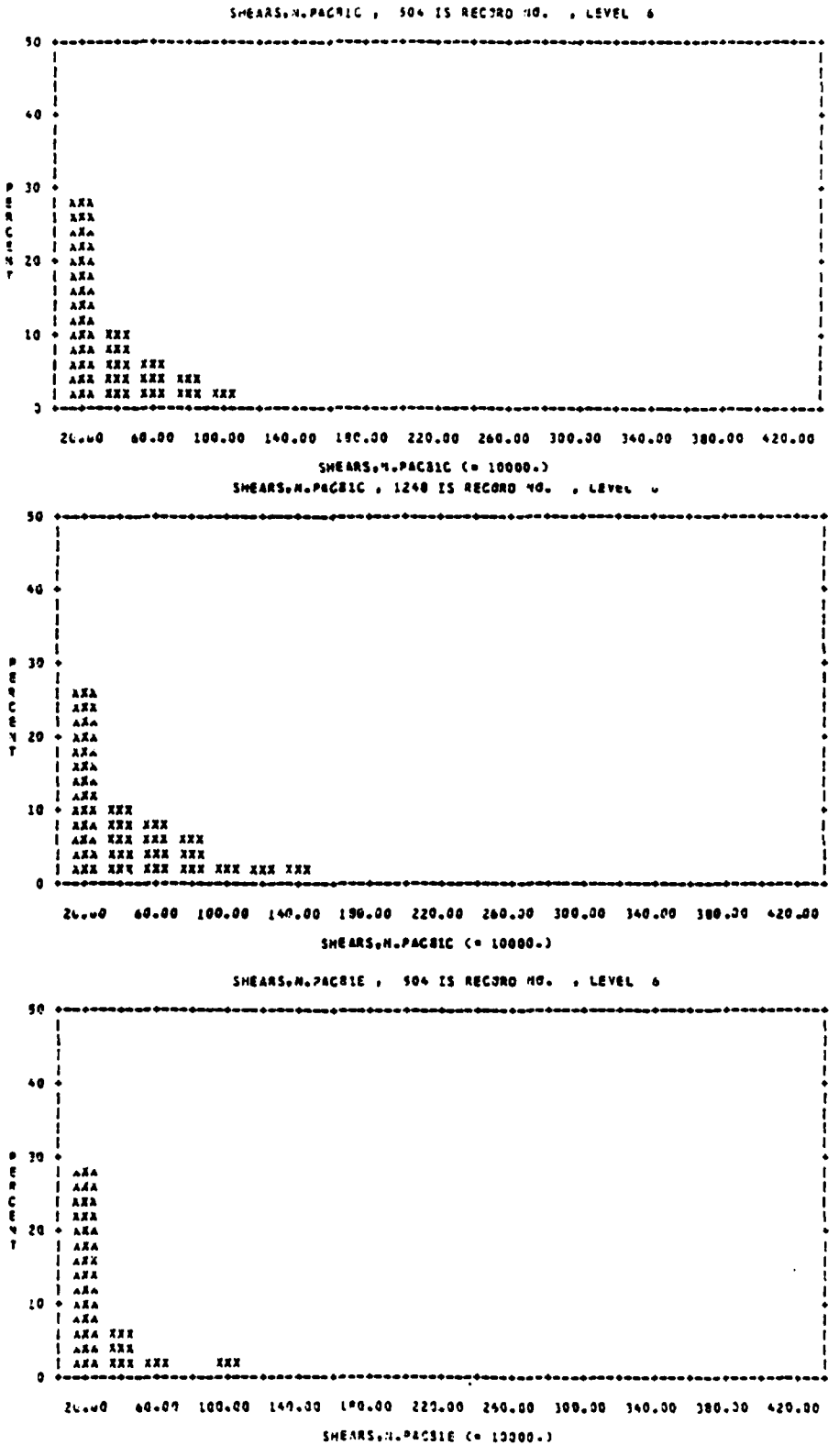

Figure 26. Frequency distribution of 32.5 m shear (s^{-1} x 10^4) for March through May.

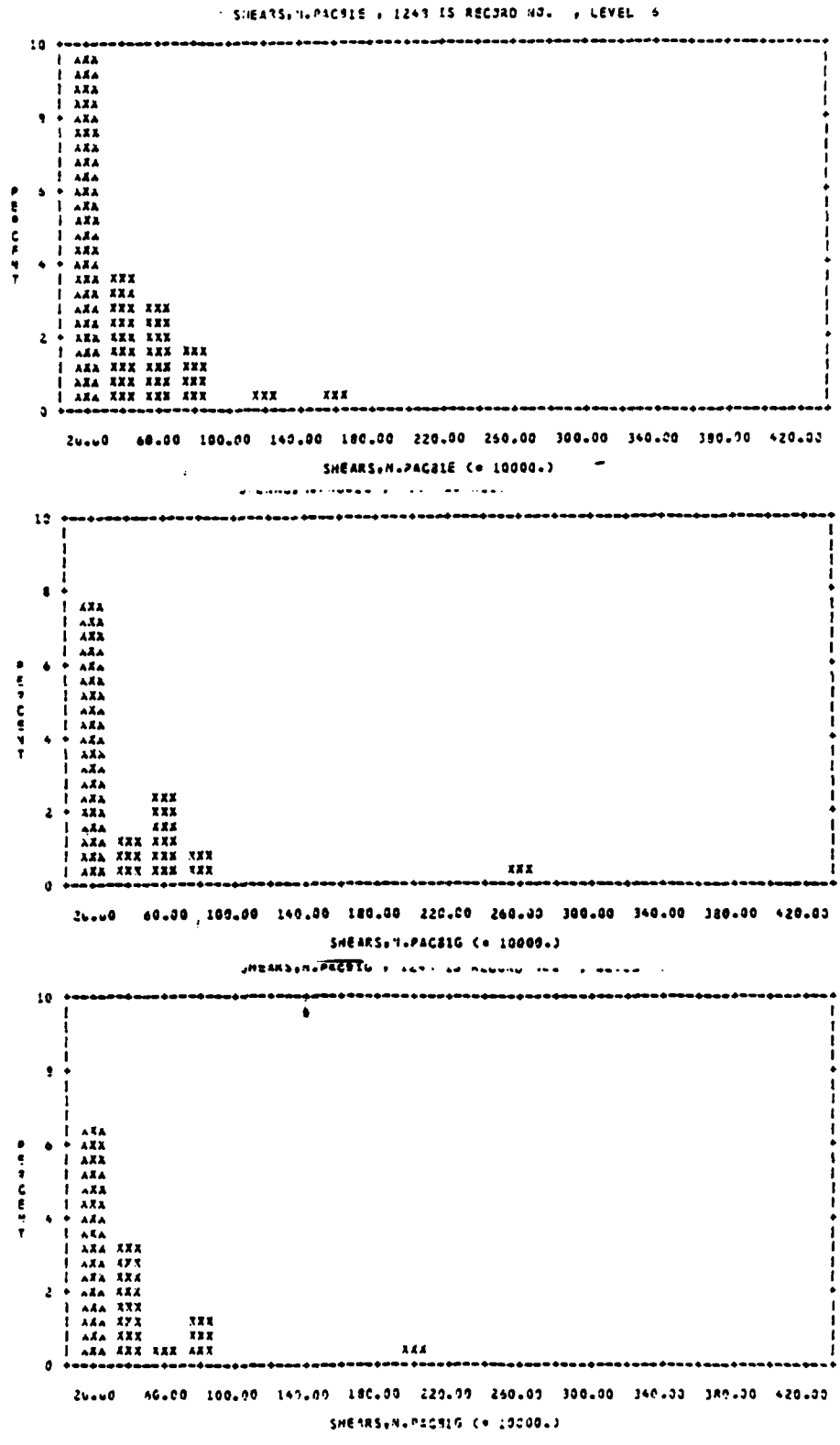

Figure 27. Frequency distribution of 32.5 m shear (s^{-1} x 10^4) for June through August.

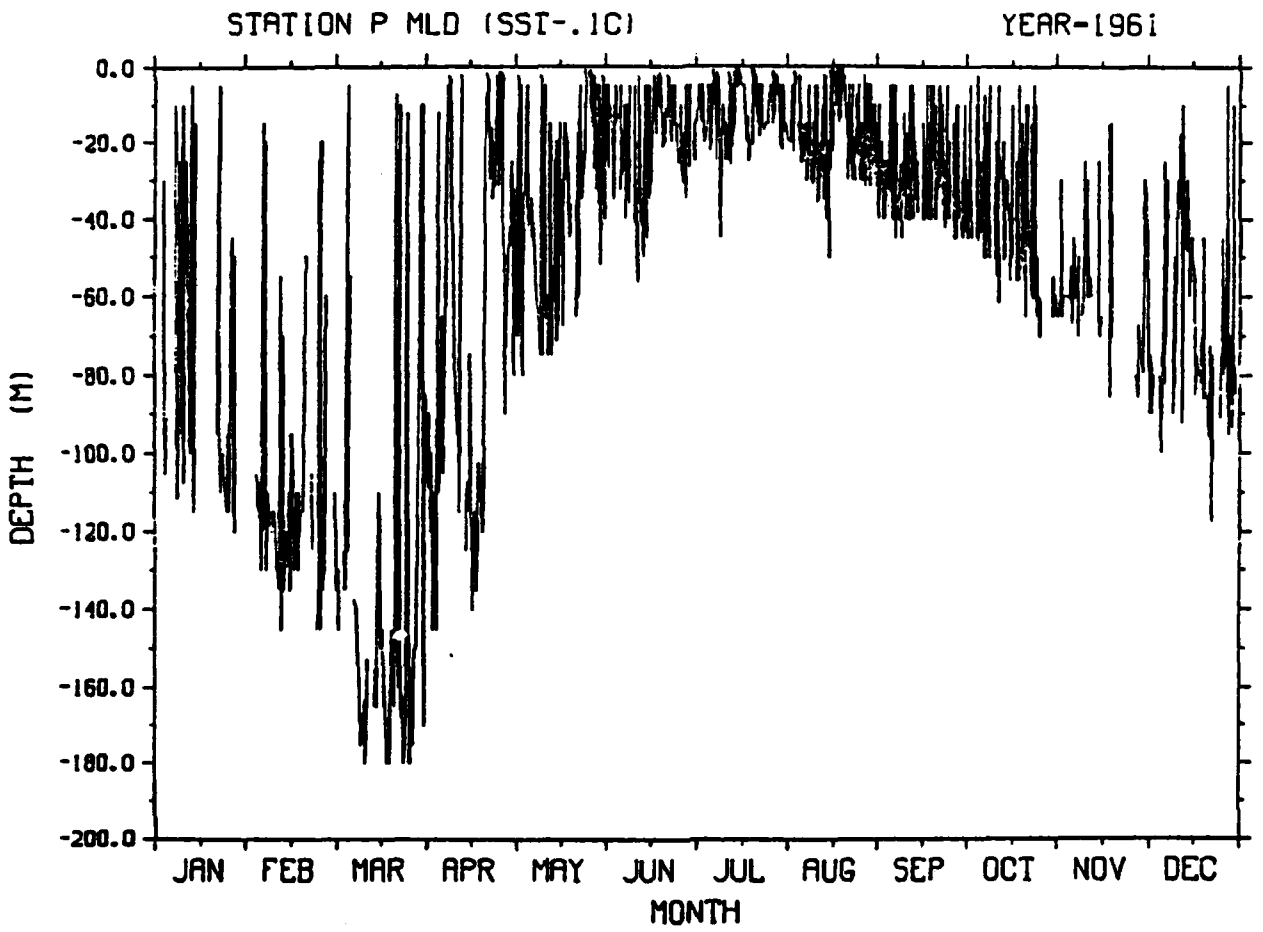

Figure 28. Ocean Station Papa mixed layer depth values for the year 1961.

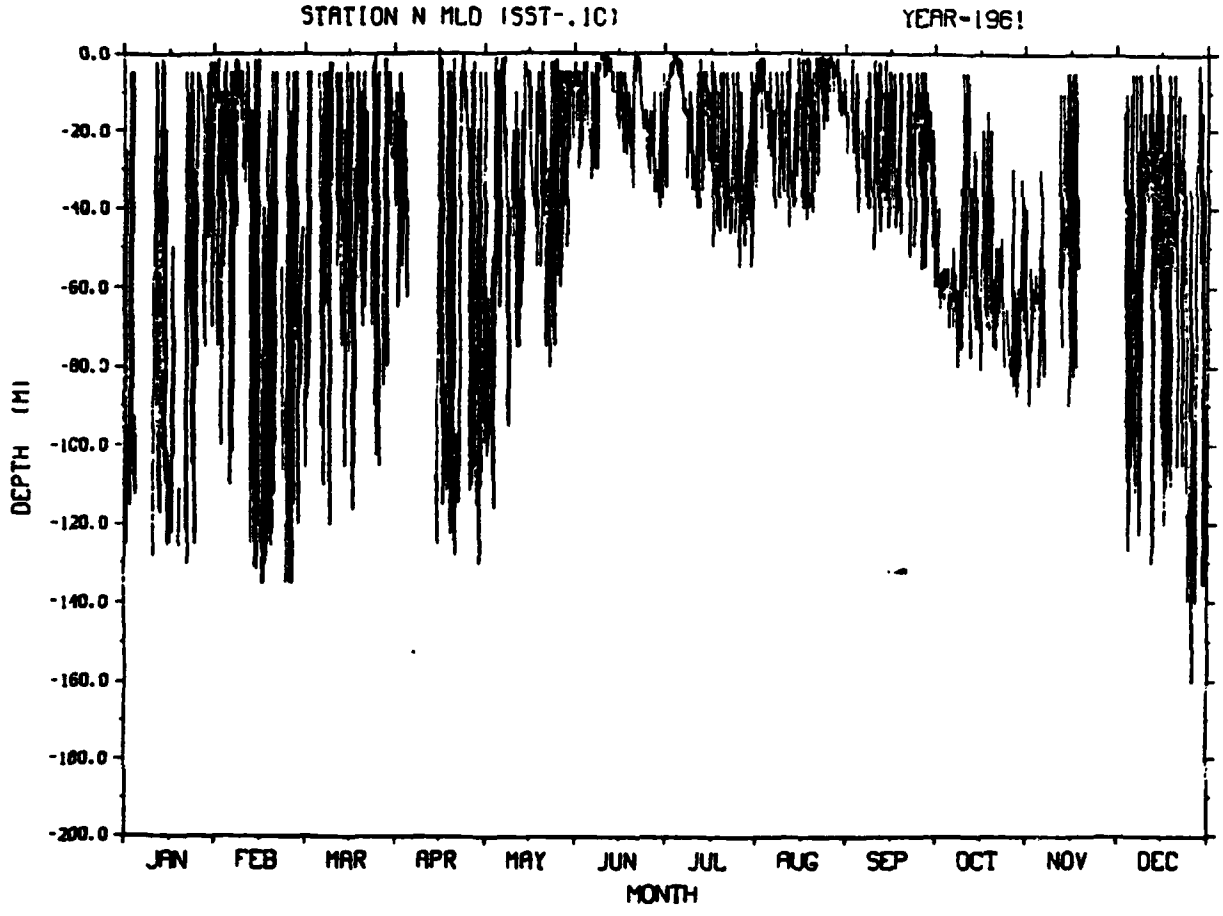

OBSERVATIONS

Figure 29. Ocean Station November mixed layer depth values for the year 1961.

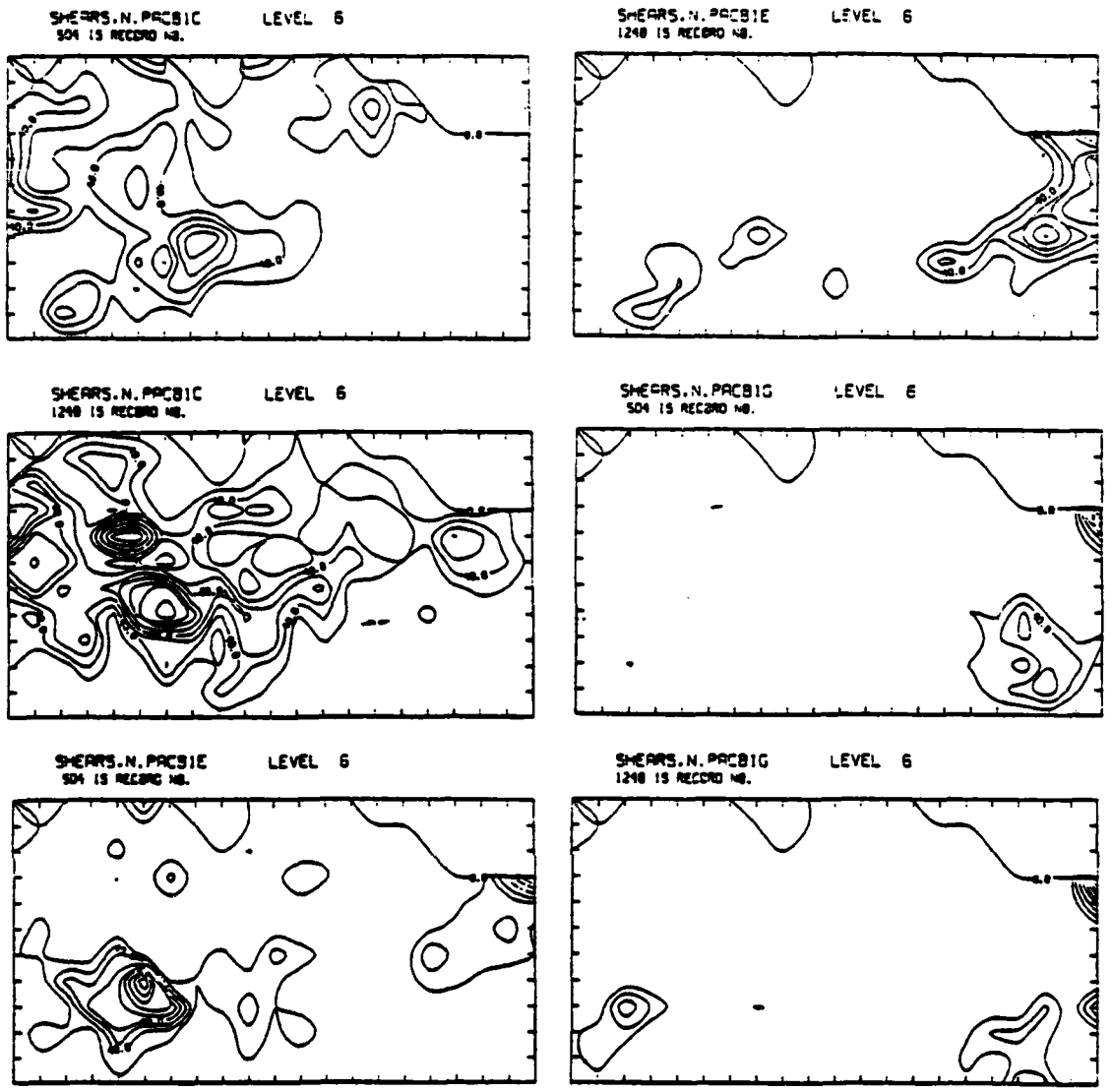

Figure 30. Monthly values of 32.5 m shear (s^{-1} x 10^4) for March through August.

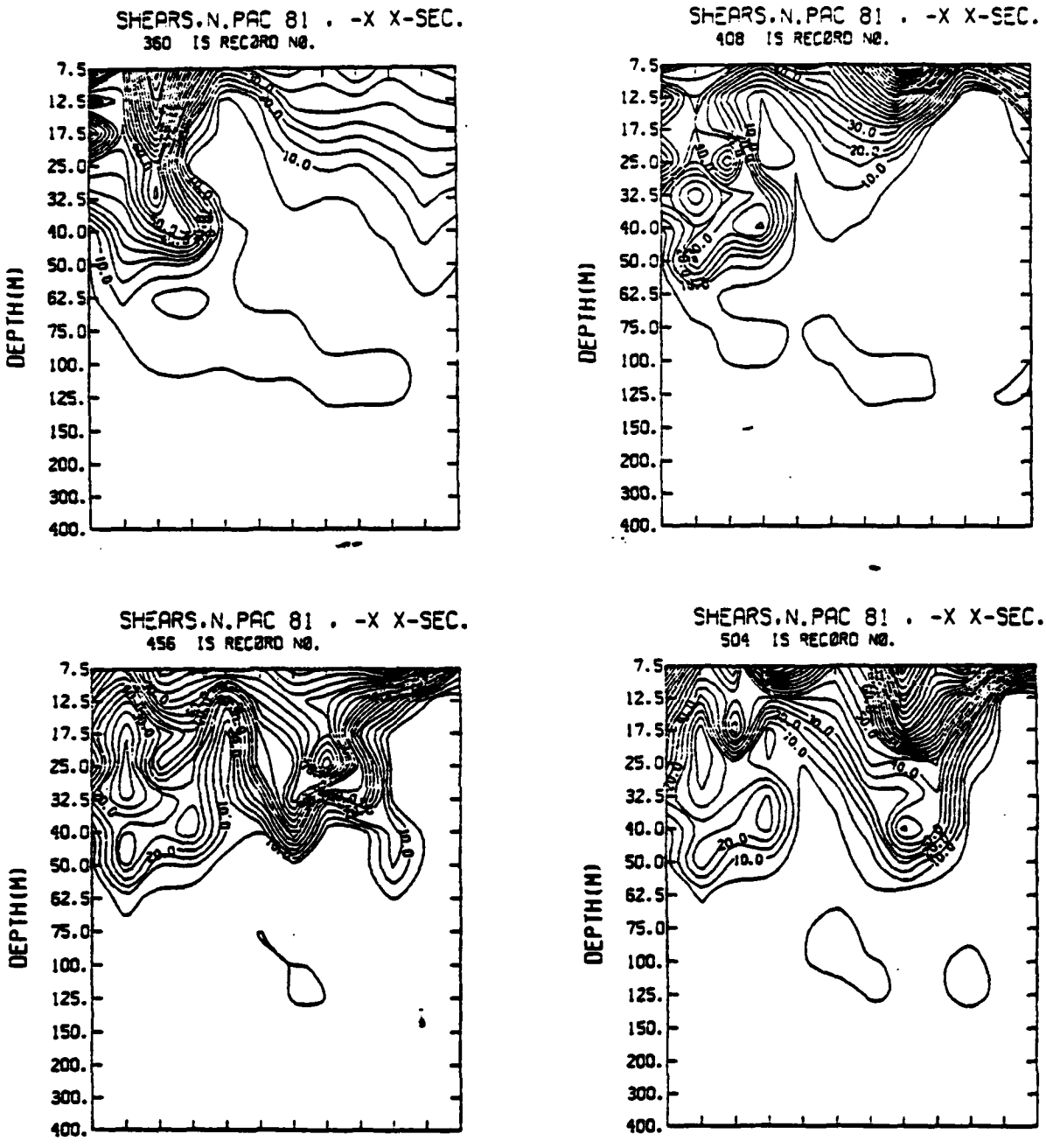

Figure 31. "Short" cross sections of shear ($s^{-1} \times 10^4$) starting at noon of March 17 and continuing for 48 hour intervals through noon of March 23.

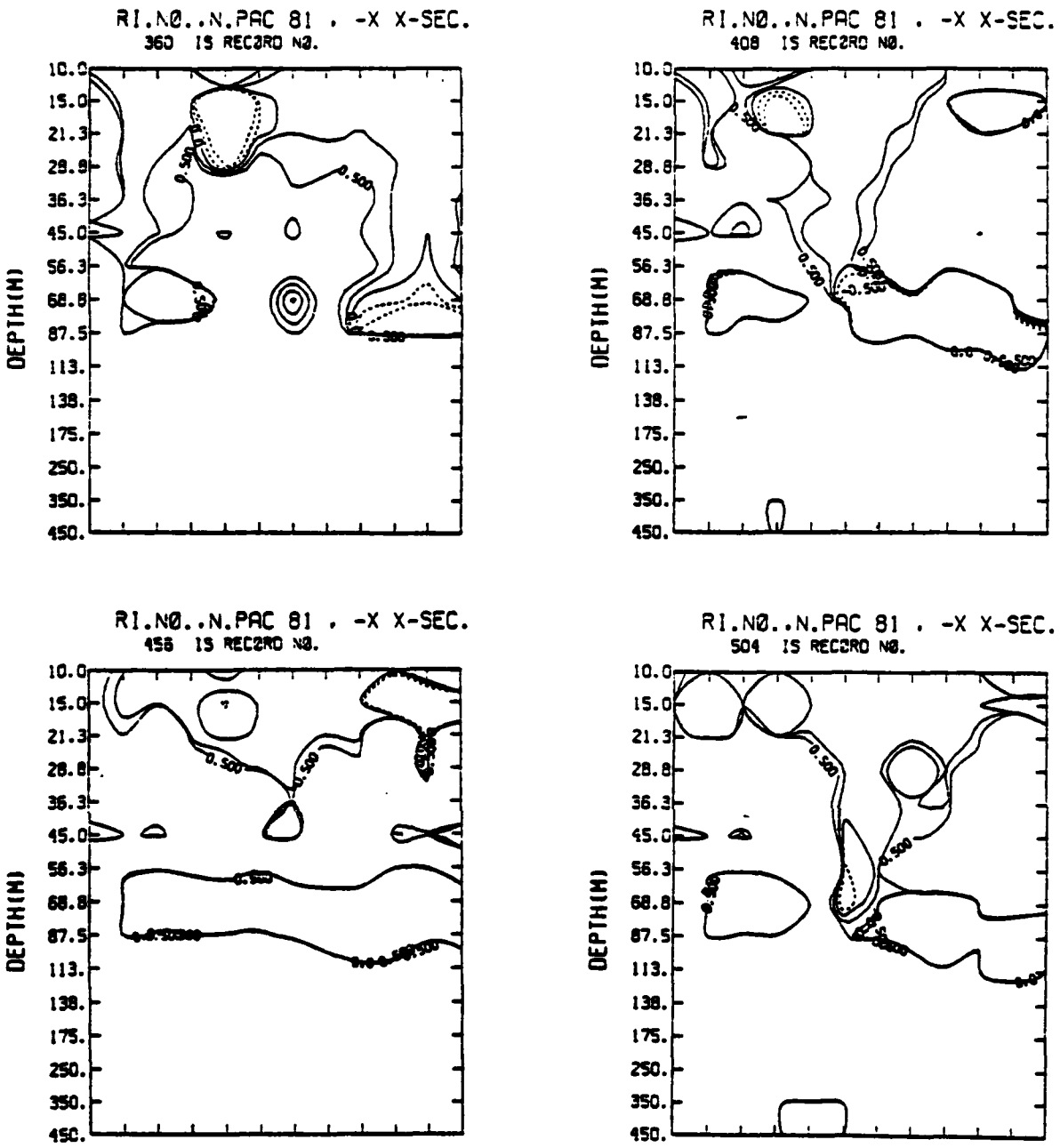

Figure 32. "Short" cross sections of Richardson number for the same time period as that of Figure 31.

represents Richardson numbers for this same time period. These show the region of instability extending down to approximately 100 m depth. These two figures show how closely regions of instability correspond to regions of shear. Figure 33 shows the same time series of shear for April (16-22). Values of shear extend to approximatley 60 m depth, having shallowed somewhat from their March position. Richardson number cross sections (Figure 34) for this period show the development of an interesting feature, two vertically separate regions of instability. The shallower region extends from the surface to 25 m depth while the deeper region exists at an average depth of 80 m. This secondary deep instability is a remnant of the deeply mixed layer which existed in March.

In our previous study of shear, a strong correlation existed between frontal passage and dynamic stability of the mixed layer. Halpern (1974) saw the same correlation from moorings in the northeastern Pacific. Figures 35 and 36 are examples of fronts overlain on Richardson number plots calculated at 10 m depth in March and April. Most of the area in these figures represents a Richardson number between 0-.25. Regions of frontal passage are related to Richardson number values between 0-.25 while values greater than .25 are found in regions of high pressure systems.

Figures 37 and 38 show histograms of Richardson number at 10 m for the thirty day intervals presented in Figure 20. Once again, note the differences of scales on the y-axis. The percentage of Richardson number lying between 0-.25 drops dramatically in June, July and August.

A seasonal comparison of shear is depicted in the following figures. A sixty day TOPS model run, initialized at October 29, 1980, was conducted for November and December of 1980. Solutions at noon of November 13, 15, 17 and 19 are presented in comparison with solutions at noon of May 16, 18, 20 and 22. Horizontal cross sections at 7.5 m, Figures 39 and 40, for these two time periods show that shear near the surface is higher during the spring then during the fall. In the upper left hand corner of these plots, that region south-southwest for the

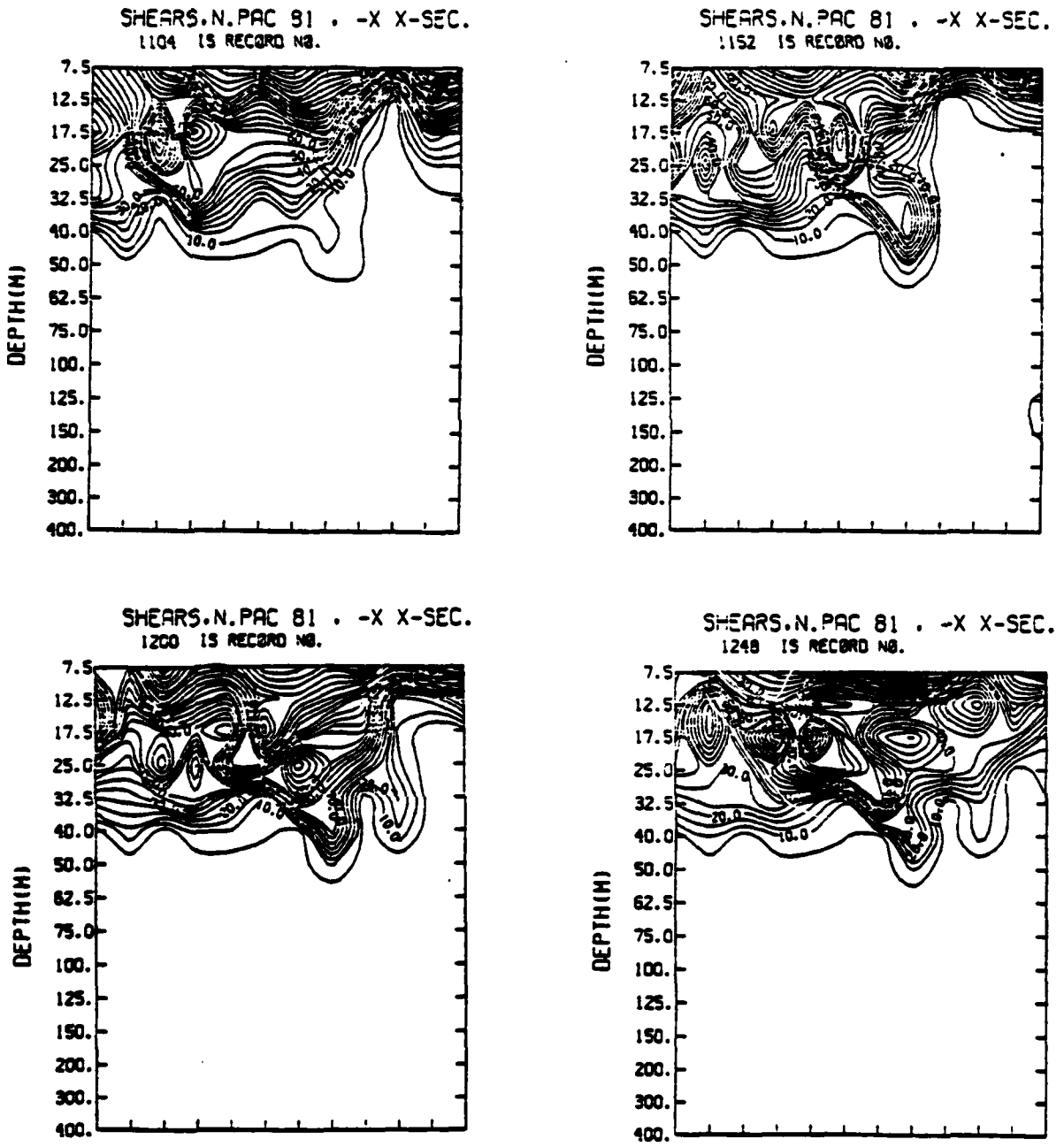

Figure 33. "Short" cross sections of shear ($s^{-1} \times 10^4$) starting at noon of April 16 and continuing at 48 hour intervals through noon of April 22.

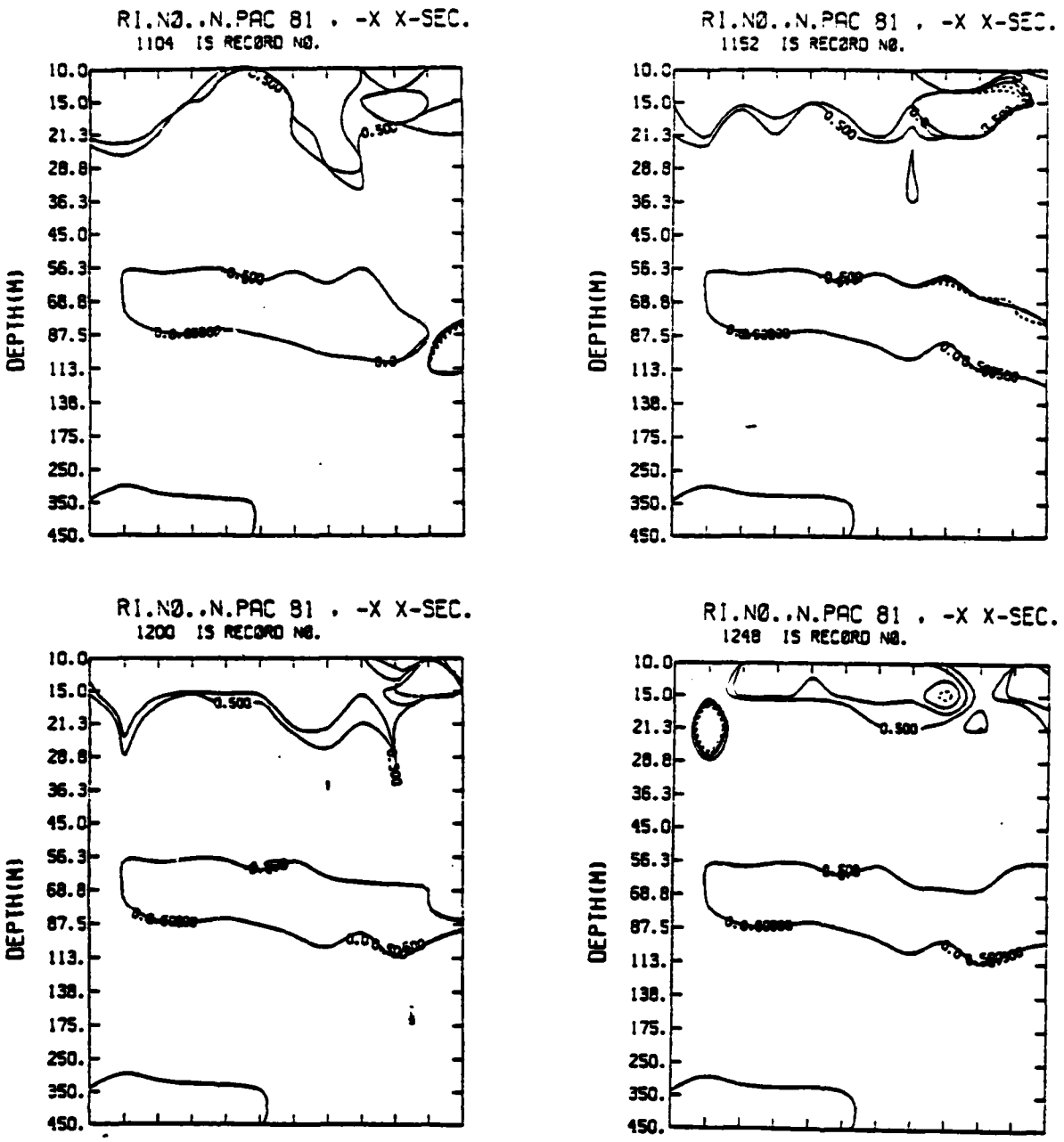

Figure 34. "Short" cross sections of Richardson number for the same time period as that of Figure 33.

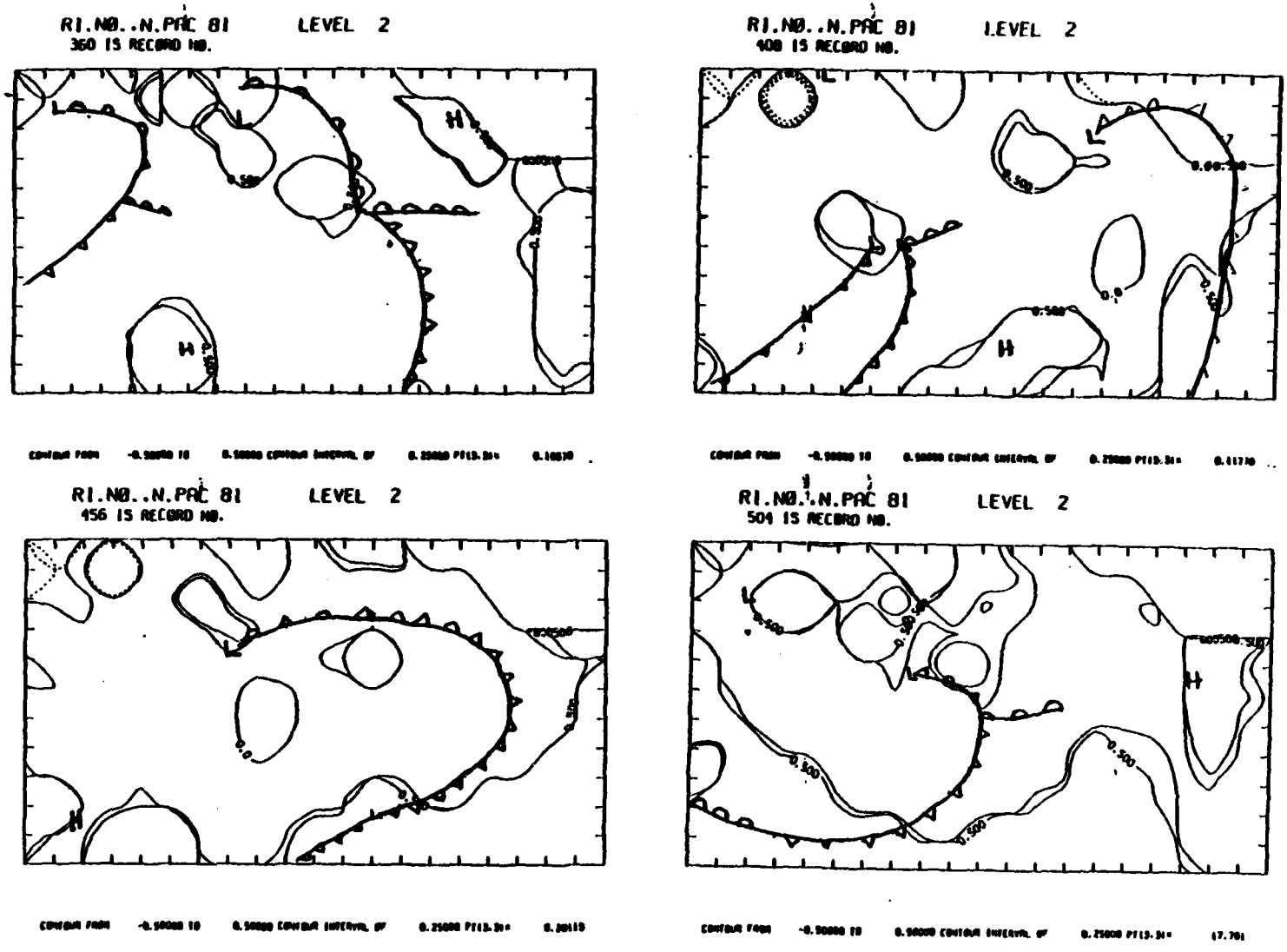

Figure 35. Level 2 (7.5 m) Richardson number plots with atmospheric fronts overlaid for the same time period as Figure 31.

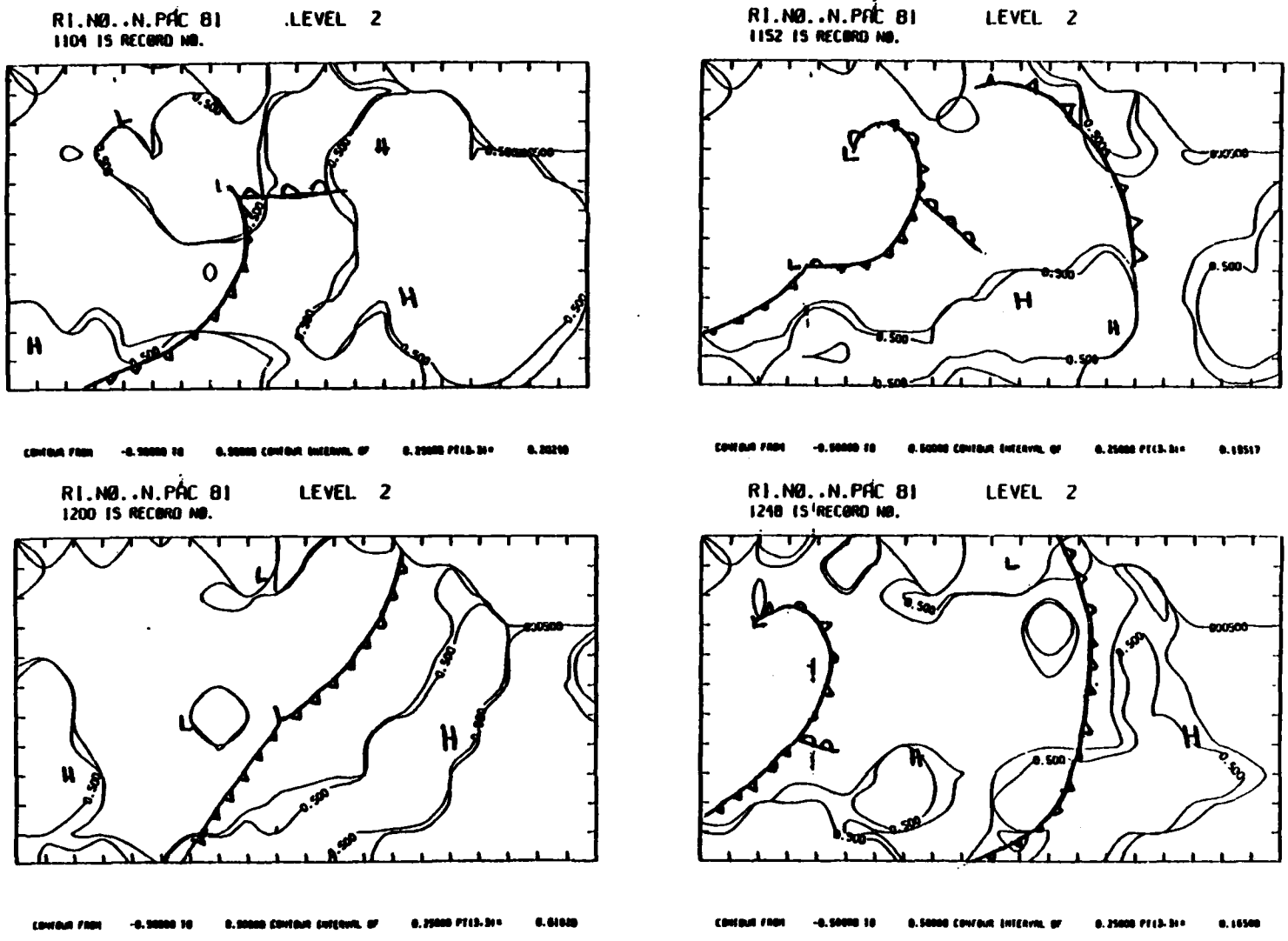

Figure 36. Level 2 (7.5 m) Richardson number plots with atmospheric fronts overlaid for the same time period as Figure 33.

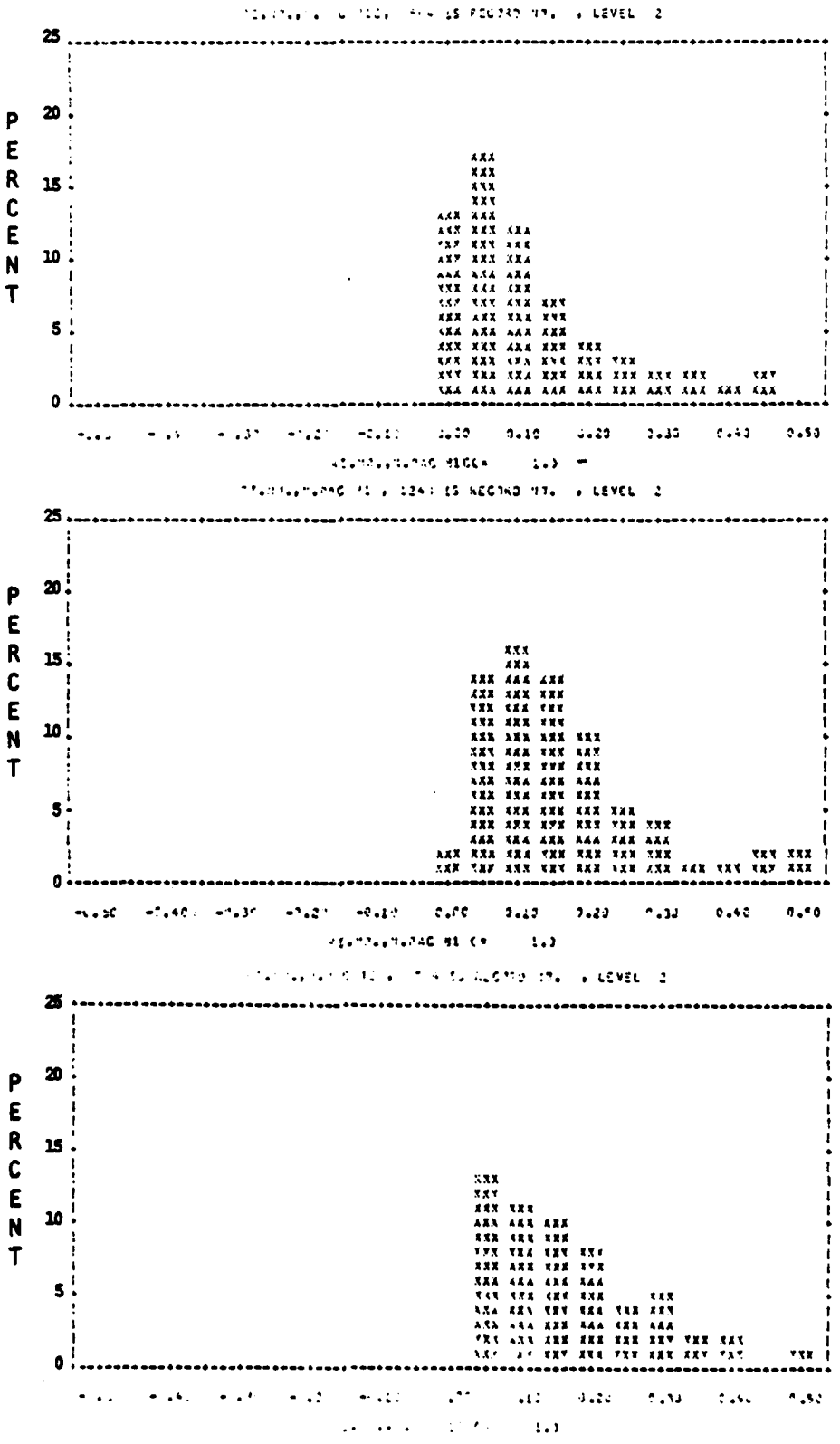

Figure 37. Monthly Level 2 (7.5 m) Richardson number frequency distribution for March through May.

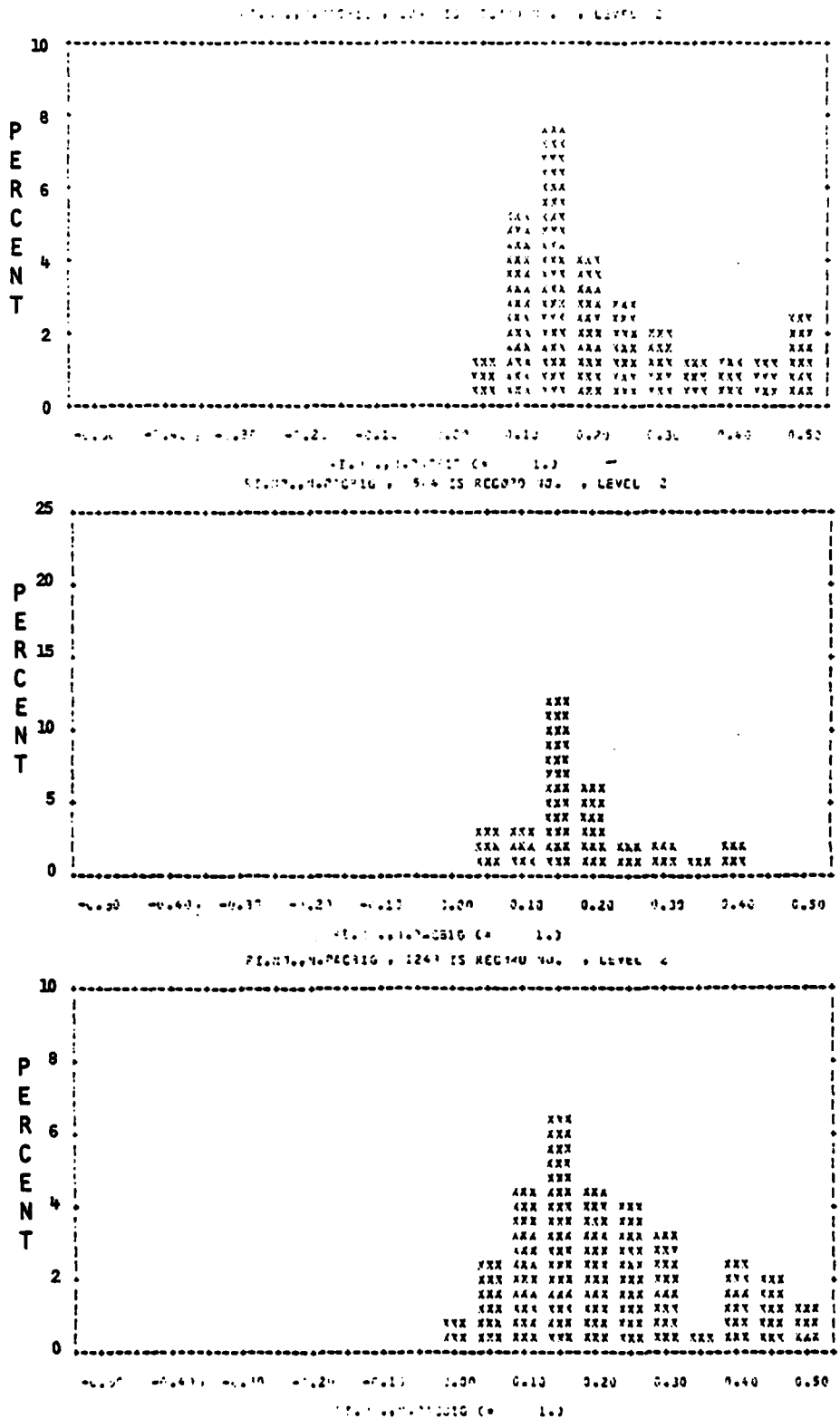

Figure 38. Monthly Level 2 (7.5 m) Richardson number frequency distribution for June through August.

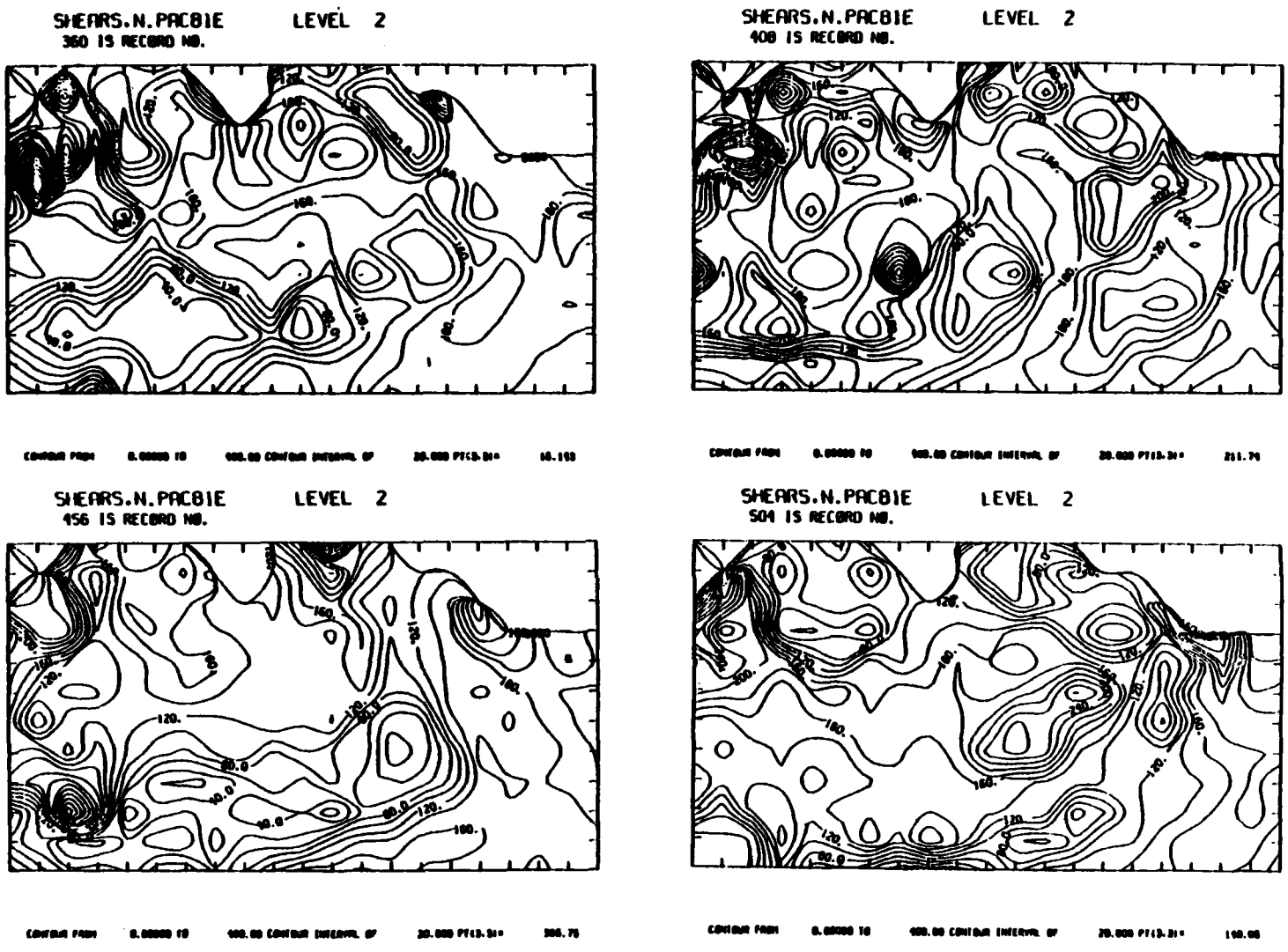

Figure 39. Level 2 (7.5 m) shear (s^{-1} x 10^4) at 48 hour intervals beginning at noon on May 16 through noon on May 22.

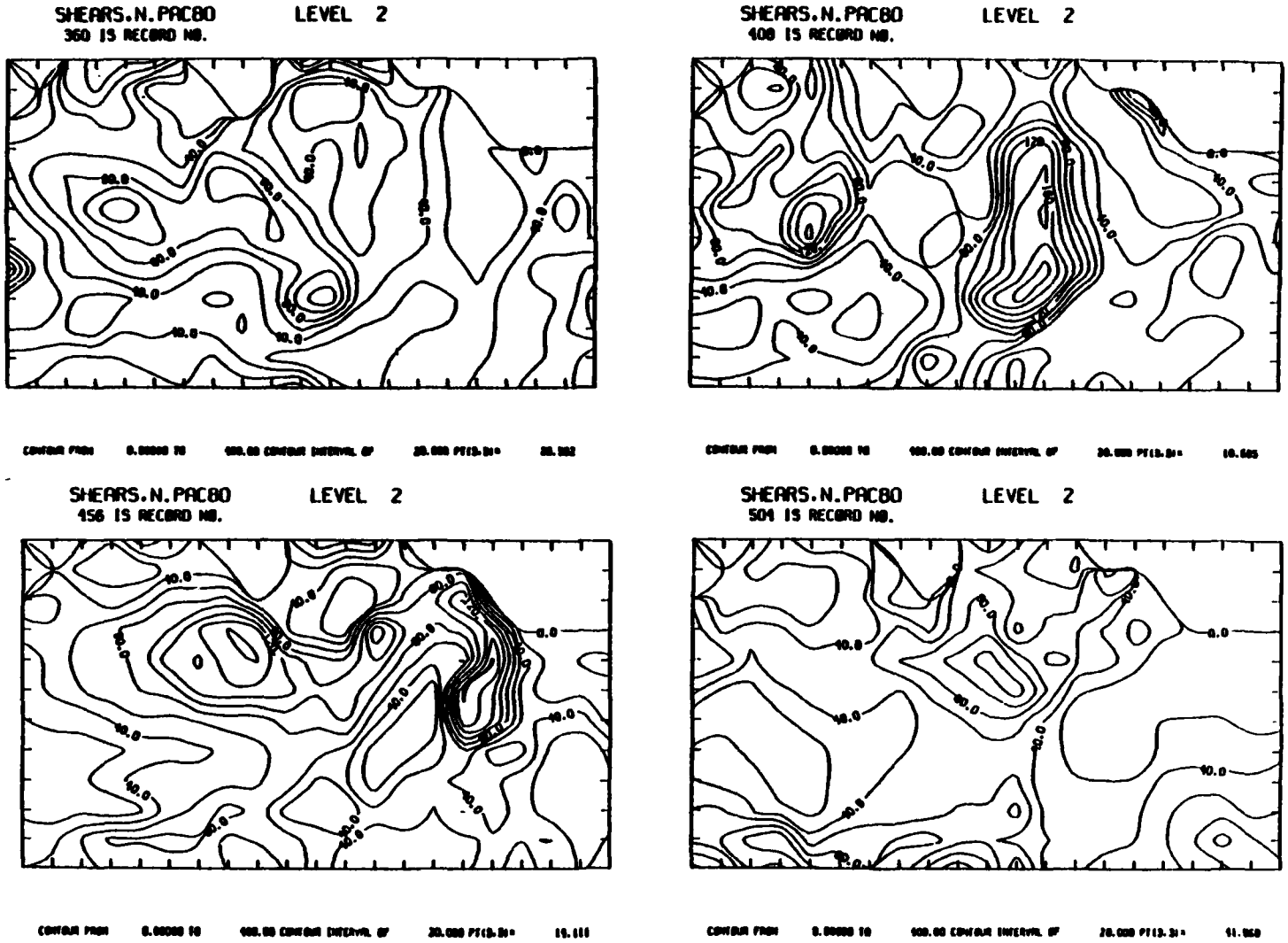

Figure 40. Level 2 (7.5 m) shear (s^{-1} x 10^4) at 48 hour intervals beginning at noon on November 13 through noon on November 19.

Bering Sea values of shear are twice as large in May as in November. The vertical cross sections, Figures 41, 42, 43 and 44 also indicate that shear is higher in spring than fall, and deeper in fall than spring. This comparison agrees with the mixed layer depths at stations Papa and November. Both of these stations indicated that the mixed layer depth is greater in November than in May. Solutions at an average depth of 32.5 m (level 6) for both seasons, Figures 45 and 46, compare quite closely.

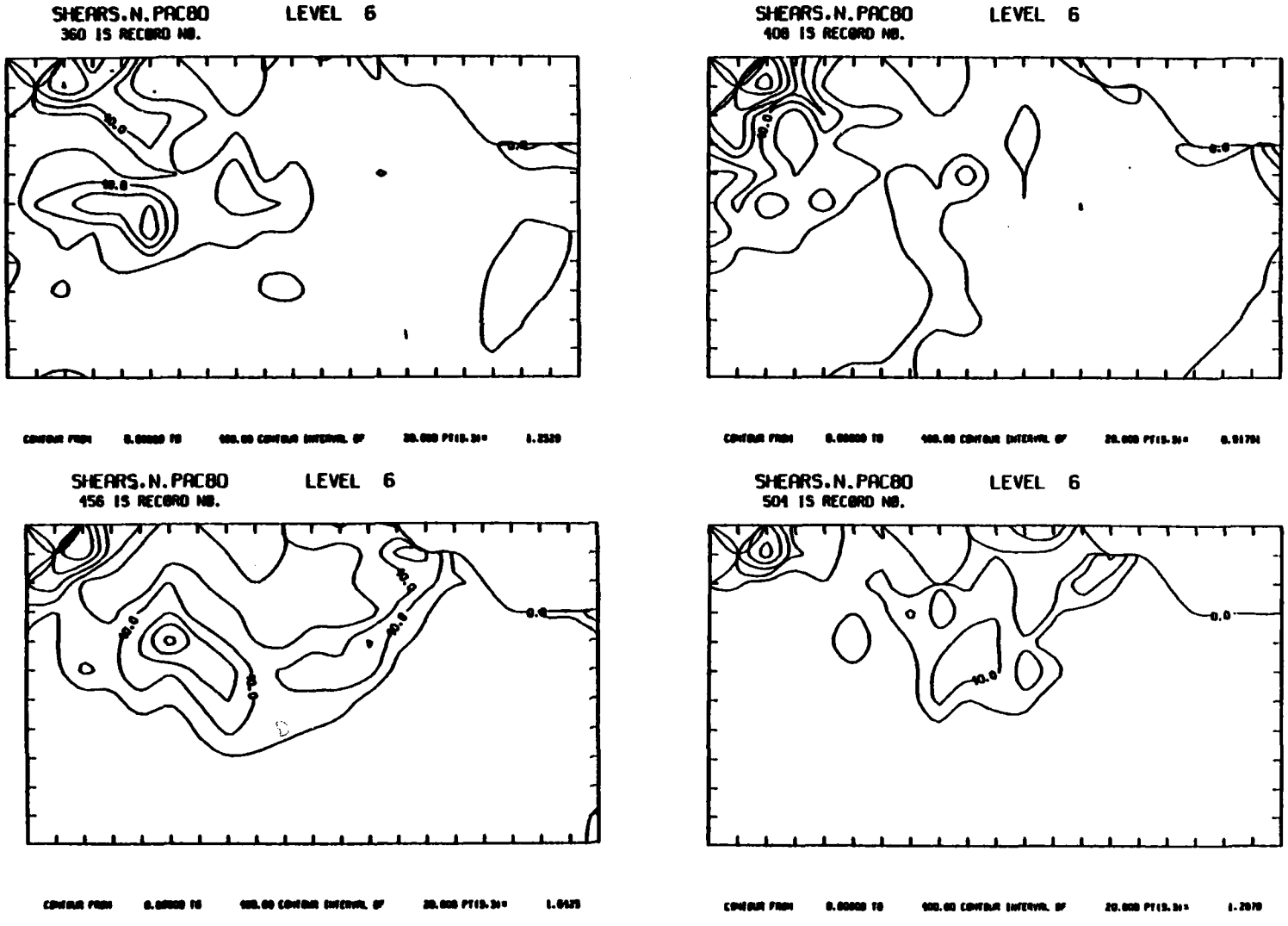

Figure 41. "Short" cross sections of shear (s^{-1} x 10^4) for the 48 hour intervals beginning at noon on May 16 through noon on May 22.

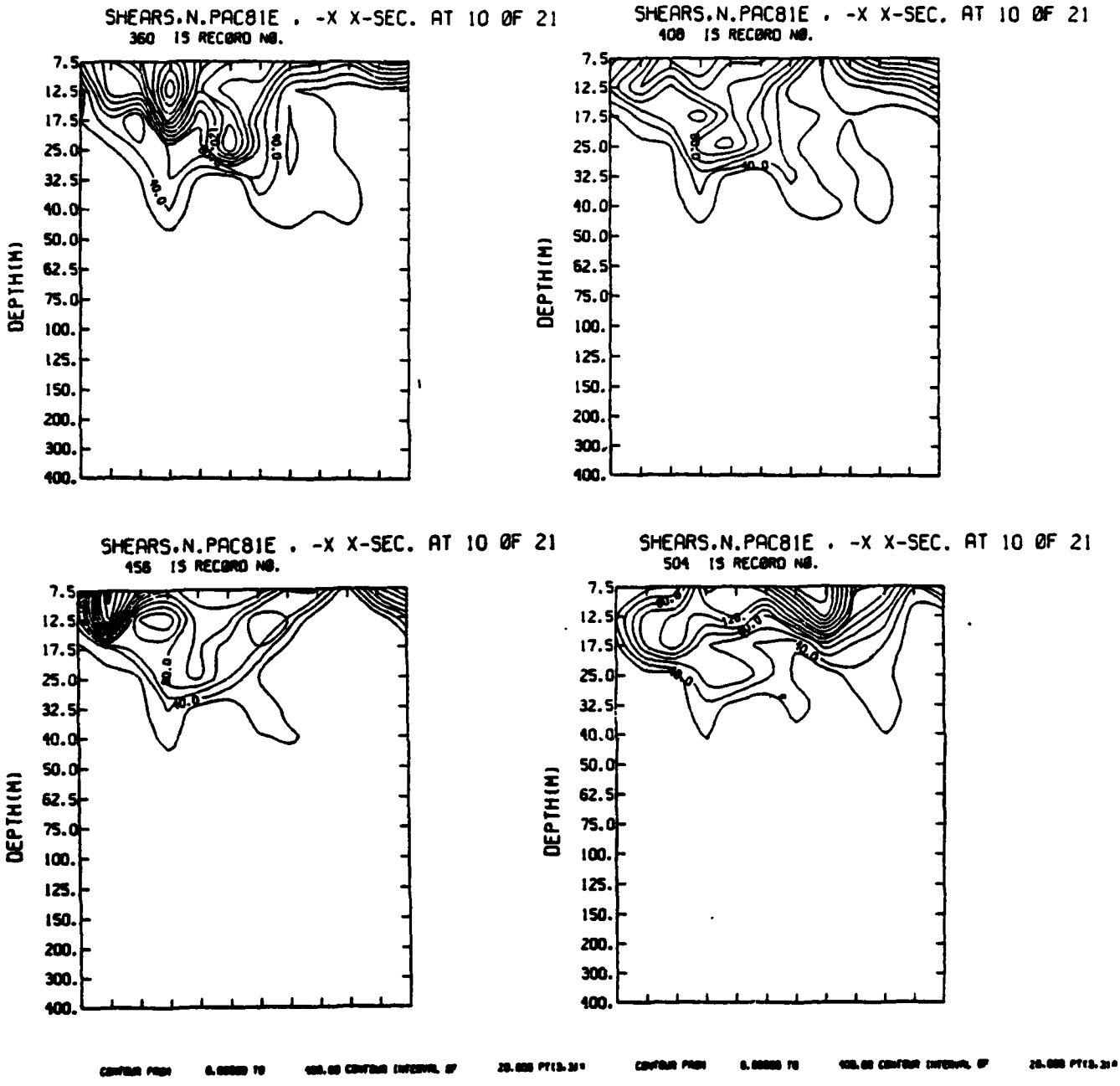

Figure 42. "Short" cross sections of shear (s^{-1} x 10^4) for the 48 hour intervals beginning at noon on November 13 through noon on November 19.

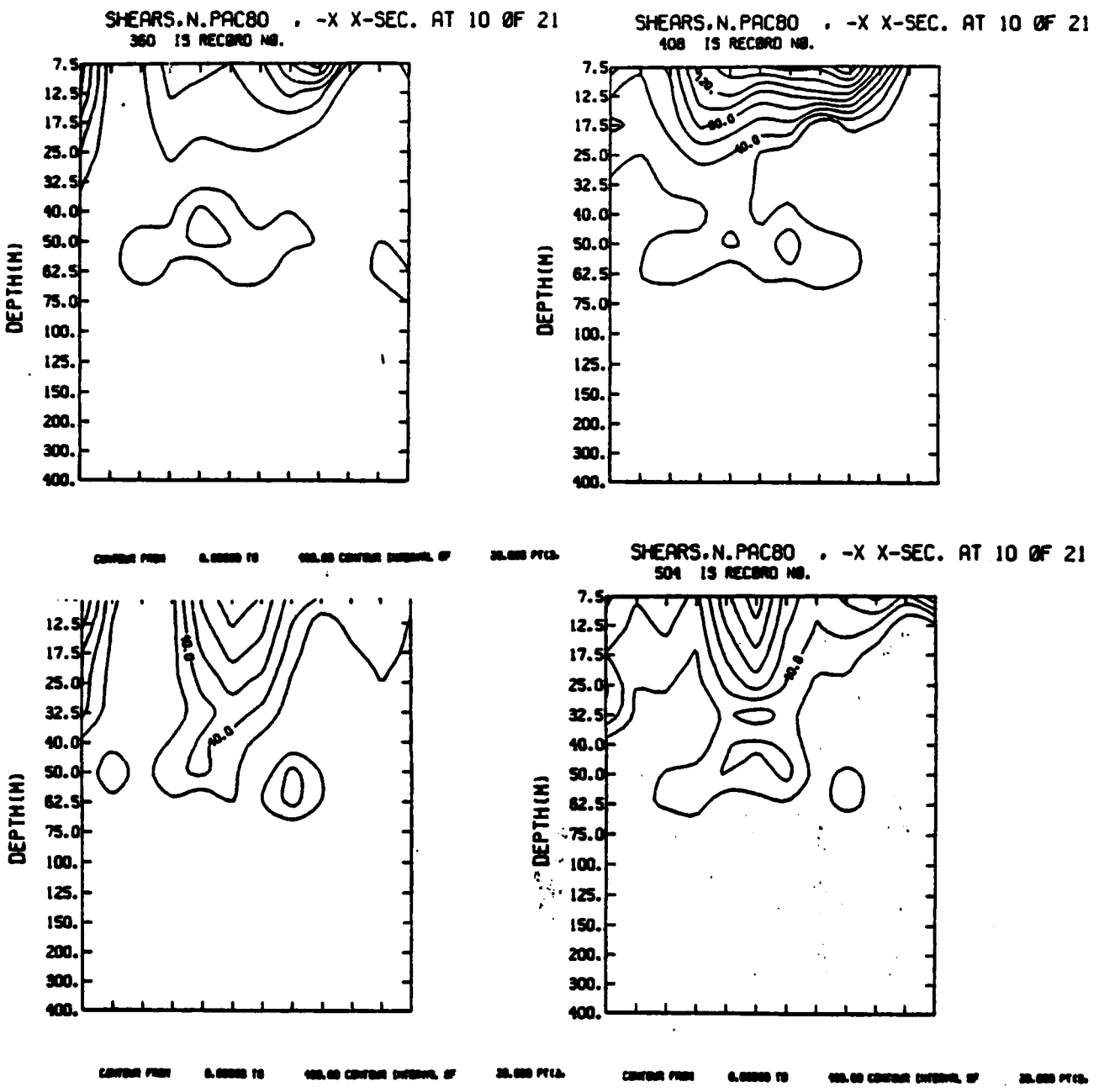

Figure 43. "Long" cross section of shear (s^{-1} x 10^4) for the 48 hour intervals beginning at noon on May 16 through noon on May 22.

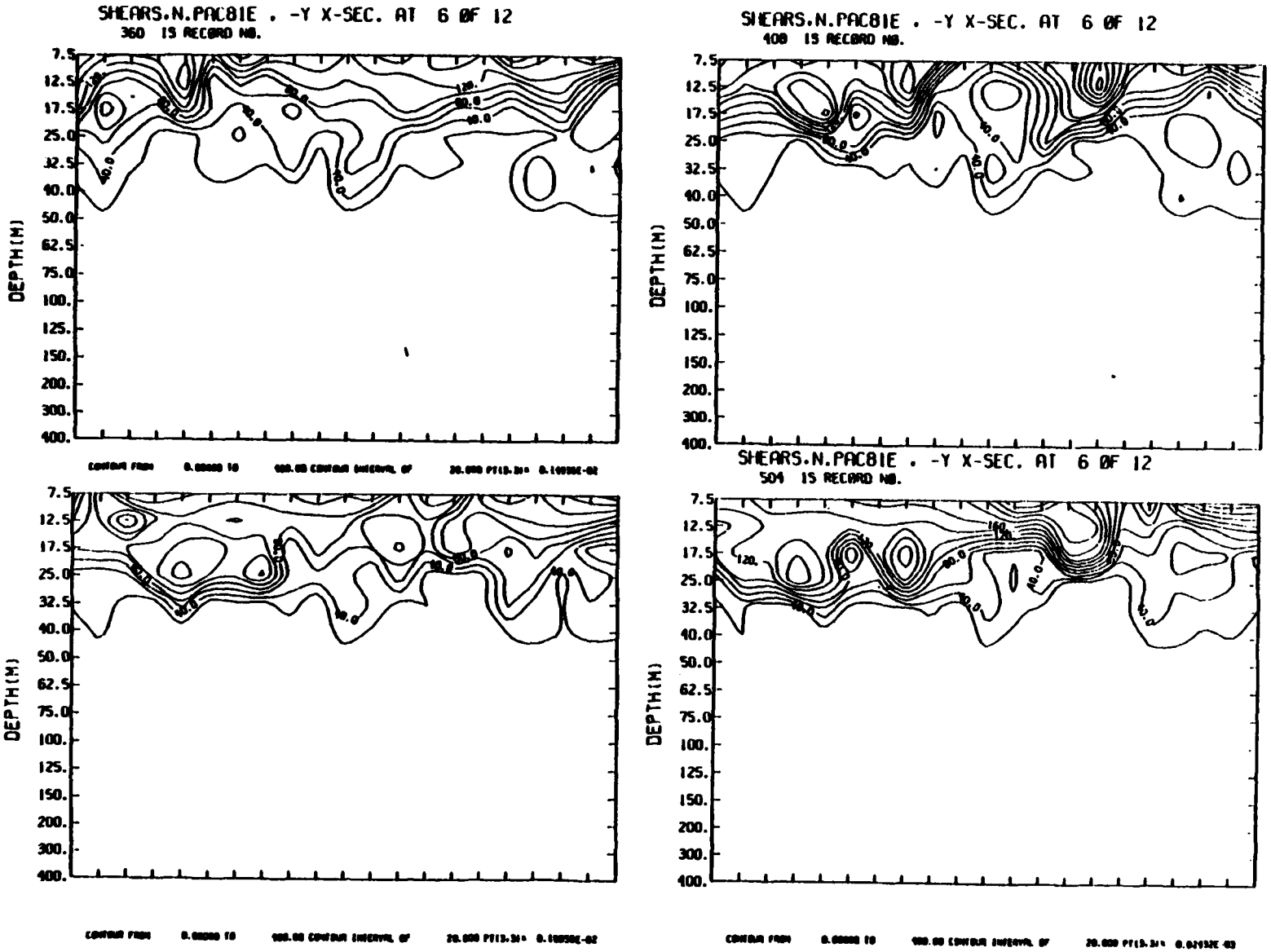

Figure 44. "Long" cross section of shear (s^{-1} x 10^4) for the 48 hour intervals beginning at noon on November 13 through noon on November 19.

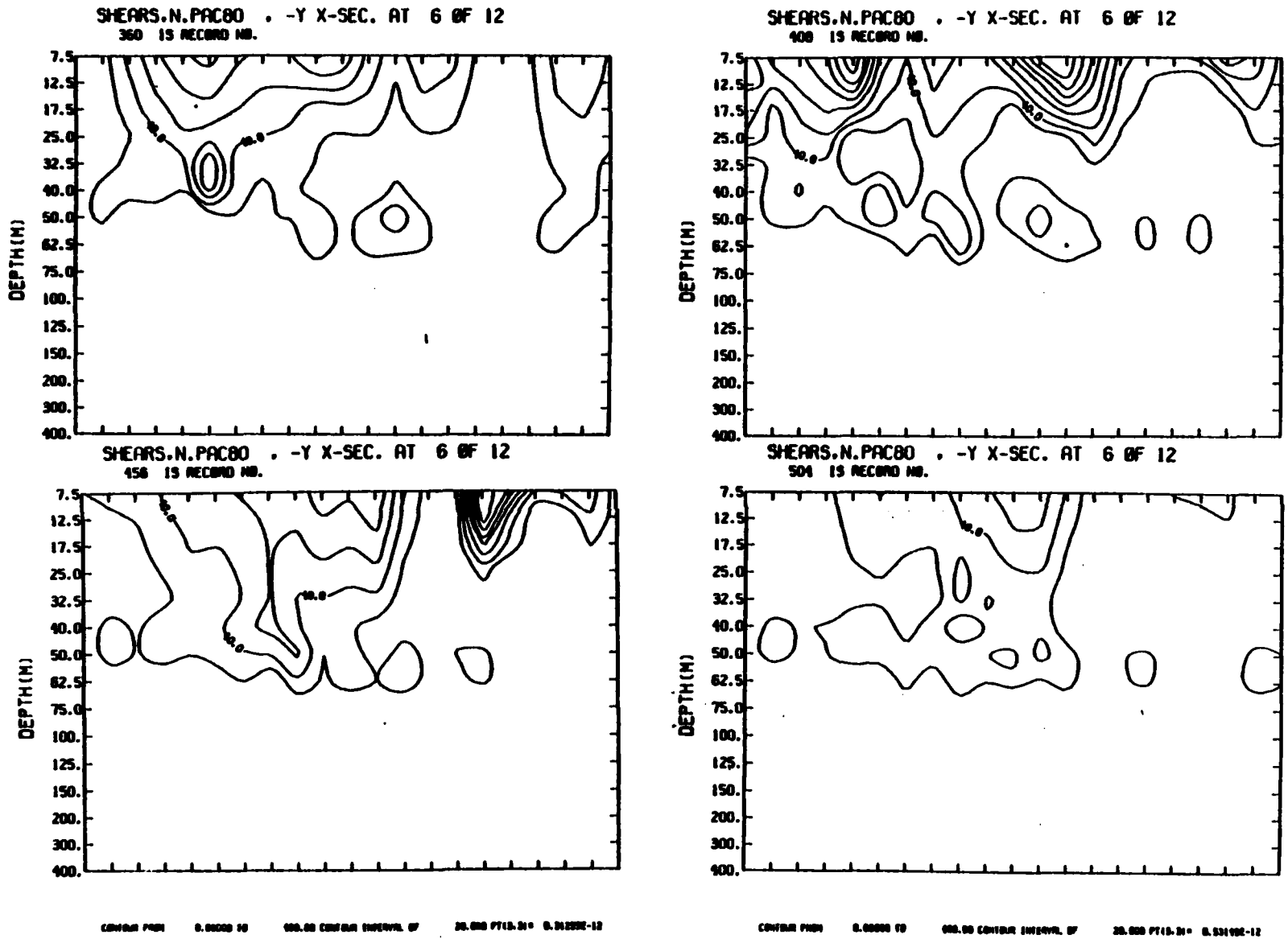

Figure 45. Level 6 (32.5 m) shear (s^{-1} x 10^4) for noon of May 16 through noon of May 22.

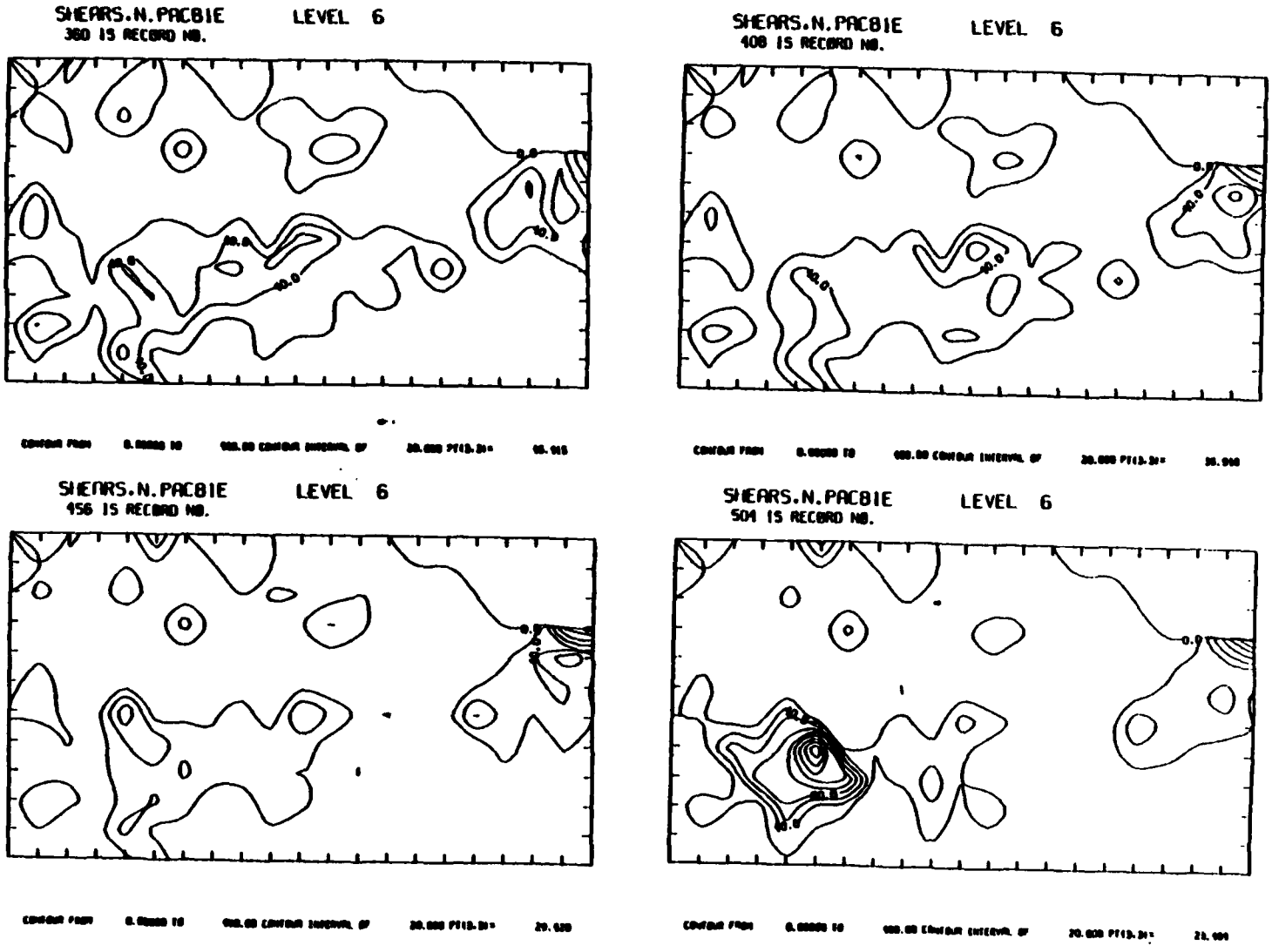

Figure 46. Level 6 (32.5 m) shear (s^{-1} x 10^4) for noon of November 13 through noon of November 19.

SUMMARY AND CONCLUSIONS

This study has attempted to simulate the statistics of temporal and geographical distribution of shear over the upper 400 m of the world's oceans. In particular we have examined a large area of the North Pacific over the six month period March through August of 1981. Forcing was provided by the prediction fields obtained from FNOC's hemispheric weather model.

Model results have shown:

- Surface shear increases from late winter - early spring to summer.
- The region south-southwest of the Bering Sea develops into a region of very high surface shear in spring and summer.
- The depth to which shear extends is closely correlated to the mixed layer depth, thus in winter shear values are found at greater depths then in summer.
- Seasonal comparisons show that the magnitude of shear is larger in May then in November, but extends to greater depths in November then in May.
- Shear instability is strongly linked to the passage of atmospheric fronts. Regions of stability occur under high pressure systems and low winds.
- Very little convective instability exists during the six month period examined ($R_f < 0$).

REFERENCES

Clancy, R. M. and P. J. Martin, 1979: The NORDA/FLENUMOCEANCEN thermodynamical ocean prediction system (TOPS): A technical description. NORDA Tech. Note 54, 28 p.

Clancy, R. M. and P. J. Martin, 1981: Synoptic forecasting of the oceanic mixed layer using the Navy's operational environmental data base: Present capabilities and future applications; Bull. Amer. Met. Soc. 62, p 770-784.

Clancy, R. M., P. J. Martin, S. A. Piacsek and K. Pollak, 1981: Test and evaluation of an operationally capable synoptic upper-ocean forecast system. NORDA Tech. NOte 92, 66 p.

Clancy, R. M. and K. Pollak, 1983: A real-time synoptic ocean thermal analysis/forecast system. Progress in Oceanography, No. 4, 1983.

Halpern, D., 1974: Observations of the deepening of the wind-mixed layer in the northeast Pacific Ocean, J. Phys. Oceanogr., 4, p. 454-466.

Harding, J. M., R. H. Preller and s. A. Piacsek, 1983: Statistics of vertical shear from a global mode. NORDA Tech. Note (#?).

Martin, P. J., 1982: Mixed layer simulation of buoy observations taken during Hurricane Eloise, J. Geophys. Res., 87, p. 409-427.

Martin, P. J., 1983: Simulation of the mixed layer at ocean weather station November and Papa with several models. NORDA Tech. Report (in preparation).

Mellor, G. L. and T. Yamada, 1974: A hierarchy of turbulence closure models for planetary boundary layers, J. Atmos. Sci., 31, p. 1791-1806.

Warn-Varnas, A. C., R. M. Clancy, M. L. Morris, P. J. Martin, S. Horton, 1983: Studies of large-scale thermal variability with a synoptic mixed layer model, NORDA Tech. Note 156, 34 p.

Warn-Varnas, A. C. and G. Dawson, 1981: An analysis of modeled shear distribution during MILE. NORDA Tech. Note 84, 36 p.

Warn-Varnas, A. C. and G. Dawson, and P. J. Martin, 1981: Forecast and studies of the oceanic mixed layer during the Mile experiment, Geophys. Astrophys. Fluid Dyn., 17, p 63-85.

Yamada, T., 1975: The critical Richardson number and the ratio of the eddy transport coefficients obtained from a turbulence closure model. J. Atmos. Sci., 32, p. 926-933.

END

FILMED

10-83

DTIC